Cellular/Molecular

The Ca_v3–K_v4 Complex Acts as a Calcium Sensor to Maintain Inhibitory Charge Transfer during Extracellular Calcium Fluctuations

Dustin Anderson,* Jordan D. T. Engbers,* N. Colin Heath, Theodore M. Bartoletti, W. Hamish Mehaffey, Gerald W. Zamponi, and Ray W. Turner

Hotchkiss Brain Institute, University of Calgary, Calgary, Alberta T2N 4N1, Canada

Synaptic transmission and neuronal excitability depend on the concentration of extracellular calcium ($[Ca]_o$), yet repetitive synaptic input is known to decrease $[Ca]_o$ in numerous brain regions. In the cerebellar molecular layer, synaptic input reduces $[Ca]_o$ by up to 0.4 mM in the vicinity of stellate cell interneurons and Purkinje cell dendrites. The mechanisms used to maintain network excitability and Purkinje cell output in the face of this rapid change in calcium gradient have remained an enigma. Here we use single and dual patch recordings in an *in vitro* slice preparation of Sprague Dawley rats to investigate the effects of physiological decreases in $[Ca]_o$ on the excitability of cerebellar stellate cells and their inhibitory regulation of Purkinje cells. We find that a Ca_v3–K_v4 ion channel complex expressed in stellate cells acts as a calcium sensor that responds to a decrease in $[Ca]_o$ by dynamically adjusting stellate cell output to maintain inhibitory charge transfer to Purkinje cells. The Ca_v3–K_v4 complex thus enables an adaptive regulation of inhibitory input to Purkinje cells during fluctuations in $[Ca]_o$, providing a homeostatic control mechanism to regulate Purkinje cell excitability during repetitive afferent activity.

Introduction

The probability of transmitter release and membrane excitability of neurons is markedly influenced by calcium influx from the extracellular space. Calcium measurements have established that the resting level of $[Ca]_o$ in the brain ranges from 1.1–2.0 mM (Heinemann et al., 1977; Nicholson et al., 1978; Stöckle and ten Bruggencate, 1980), with repetitive synaptic input rapidly decreasing $[Ca]_o$ within the surrounding extracellular environment in several brain regions (Heinemann et al., 1977; Stöckle and ten Bruggencate, 1978; Egelman and Montague, 1999; Stanley, 2000; King et al., 2001; Rusakov and Fine, 2003). In the cerebellum, repetitive excitatory input quickly lowers $[Ca]_o$ by ~0.4 mM in the molecular layer (Nicholson et al., 1978; Stöckle and ten Bruggencate, 1978). Synaptically evoked decreases in $[Ca]_o$ are expected to reflect calcium influx into presynaptic terminals as well as postsynaptic cells. A prominent postsynaptic contribution to changes in $[Ca]_o$ is predicted in the molecular layer, where climbing fibers evoke a calcium-dependent complex spike that conducts throughout the Purkinje cell dendritic tree (Llinás and Sugimori, 1980b; Kitamura and Häusser, 2011). However, the effects of a decrease in $[Ca]_o$ on cell excitability or circuit function in the cerebellum has not been determined.

Stellate cells positioned within the molecular layer provide inhibitory input to Purkinje cell dendrites to suppress calcium transients associated with climbing fiber-evoked complex spikes (Callaway et al., 1995; Kitamura and Häusser, 2011). Any factor that affects stellate cell excitability then has the potential to exert considerable control over the output of the cerebellar cortex. In this regard, stellate cells express K_v4 (A-type) potassium channels that associate with potassium channel interacting protein 3 (KChIP3) (Kollo et al., 2006; Burgoyne, 2007; Anderson et al., 2010b). A protein interaction between Ca_v3 (T-type) calcium channels and K_v4 potassium channels allows Ca_v3 calcium influx and the KChIP3 subunit to regulate A-type current (I_A) in stellate cells. Specifically, Ca_v3 calcium influx invokes a depolarizing shift in the voltage dependence of I_A inactivation to decrease stellate cell excitability (Anderson et al., 2010a,b). This is important, as synaptically evoked decreases in $[Ca]_o$ in the molecular layer may affect the Ca_v3–K_v4 interaction and change stellate cell excitability.

The present study tested the hypothesis that the Ca_v3–K_v4 complex can respond to physiologically relevant decreases in $[Ca]_o$ that occur during synaptic activity to modulate cerebellar stellate cell output. We find that even subtle decreases in $[Ca]_o$ are detected by the Ca_v3–K_v4 complex to increase stellate cell gain

Received Nov. 20, 2012; revised March 21, 2013; accepted March 25, 2013.

Author contributions: D.A., J.D.T.E., W.H.M., G.W.Z., and R.W.T. designed research; D.A., J.D.T.E., N.C.H., and T.M.B. performed research; D.A., J.D.T.E., N.C.H., and T.M.B. analyzed data; D.A., J.D.T.E., G.W.Z., and R.W.T. wrote the paper.

This work was supported by grants from the Canadian Institutes of Health Research (CIHR) (R.W.T., G.W.Z.) and studentships through Alberta Innovates—Health Solutions (AIHS) (D.A., J.D.T.E. and W.H.M.), T. Chen Fong awards (D.A., J.D.T.E.), a Killam scholarship (D.A., J.D.T.E.), a CIHR-CGS PhD award (J.D.T.E.), and CIHR and AIHS postdoctoral fellowships (T.M.B.). The funders had no role in study design, data collection and analysis, decision to publish, or preparation of this manuscript. R.W.T. is an AIHS Scientist, and G.W.Z. is an AIHS Scientist and Canada Research Chair. We gratefully acknowledge D. Jaeger and R. Lin for assistance in establishing dynamic-clamp hardware and software, and M. Kruskic and L. Chen for expert technical assistance.

*D.A. and J.D.T.E. contributed equally to this work.

The authors declare no competing financial interests.

Correspondence should be addressed to Ray W. Turner, Hotchkiss Brain Institute, HRIC 1AA14, University of Calgary, 3330 Hospital Drive Northwest, Calgary, AB T2N 4N1 Canada. E-mail: rwturner@ucalgary.ca.

DOI:10.1523/JNEUROSCI.5384-12.2013

 0270-6474/13/337811-14$15.00/0

and maintain inhibitory control of Purkinje cells in the face of reduced synaptic efficacy. Moreover, the calcium-dependent decrease in stellate cell I_A is rapidly evoked by repetitive climbing fiber input, indicating an active response of the Ca_v3–K_v4 complex to physiologically relevant stimuli. The Ca_v3–K_v4 complex thus acts as a novel calcium sensor to adaptively regulate inhibitory input in relation to local changes in the extracellular milieu that accompanies repetitive synaptic input.

Materials and Methods

Animal Care. Sprague Dawley rat pups were obtained from Charles River Laboratories and maintained according to guidelines of the Canadian Council for Animal Care.

Slice preparation. Cerebellar slices were prepared from male rats of postnatal day 15 (P15) to P24. All chemicals were obtained from Sigma unless noted otherwise. Briefly, rats were anesthetized with halothane and the cerebellum removed in artificial CSF (aCSF) composed of (in mM) 125 NaCl, 3.25 KCl, 1.5 $CaCl_2$, 1.5 $MgCl_2$, 25 $NaHCO_3$, and 25 D-glucose preoxygenated by carbogen (95% O_2, 5% CO_2) gas. Parasagittal tissue slices of cerebellum (300 μm) were cut by Vibratome and transiently elevated to 34°C (60 min) before storing in carbogen-gased aCSF at room temperature. Slices were subsequently transferred to a recording chamber on a Zeiss Axioskop FS-2 microscope and maintained as a submerged preparation in oxygenated aCSF.

Heterologous expression in tsA-201 cells. The preparation of human $K_v4.2$, $Ca_v3.3$, and KChIP3 cDNAs has been described previously (Anderson et al., 2010a,b). Human DPP10c cDNA was kindly provided by P. Pfaffinger (Baylor College of Medicine, Houston, TX) and subcloned into pCDNA3.1$^-$ (Invitrogen) using XhoI/AflIII. Cells were transfected with cDNAs: $K_v4.2$ (5 μg/μl), $Ca_v3.3$ (2.5 μg/μl), KChIP3 (5 μg/μl), DPP10c (5 μg/μl), and GFP (2 μg/μl). Cells were washed with fresh media 14 h later and moved to 29°C for 2–3 d. For tsA-201 cell recordings, the extracellular solution contained (in mM) 120 NaCl, 3 $NaHCO_3$, 4.2 KCl, 1.2 KH_2PO_4, 1.5 $CaCl_2$, 1.5 $MgCl_2$, 10 D-glucose, and 10 HEPES, pH adjusted to 7.3 with NaOH. The internal solution for voltage clamp of $K_v4.2$ expressed in tSA-201 cells was as follows (in mM): 110 K-gluconate, 30 KCl, 1 EGTA, 5 HEPES, and 0.5 $MgCl_2$, pH adjusted to 7.3 with KOH.

Recording solutions. On-cell recordings for both stellate and Purkinje cells were performed with an internal electrolyte of HEPES-buffered aCSF containing the following (in mM): 150 NaCl, 3.25 KCl, 1.5 $CaCl_2$, 1.5 $MgCl_2$, 10 HEPES, and 20 D-glucose, pH 7.3 with NaOH. The internal solution for current- and dynamic-clamp whole-cell recordings was (in mM) 130 K-gluconate, 0.1 EGTA, 10 HEPES, 7 NaCl, and 0.3 $MgCl_2$, pH 7.3 with KOH, and 5 di-Tris-creatine phosphate, 2 Tris-ATP, and 0.5 Na-GTP were added from fresh frozen stock each day. Unless indicated otherwise, the internal solution for voltage-clamp recordings in stellate cells was as follows (in mM): 140 KCl, 0.1 EGTA, 10 HEPES, and 2.5 $MgCl_2$, pH adjusted to 7.3 with KOH. To isolate I_A using internal blockers, the internal solution also contained the following (in mM): 5 tetraethylammonium (TEA), 5 QX-314 bromide, 0.1 philanthotoxin, 1 MK-801, and 0.1% BSA. To isolate I_A in the presence of Ca_v3-mediated calcium current (I_T), the bathing medium contained the following (in mM): 0.0001 TTX, 5 TEA, and 2 CsCl. To isolate I_T in stellate cells during climbing fiber stimulation, the internal solution was as follows (in mM): 100 CsCl, 10 HEPES, 2.5 $MgCl_2$, 10 EGTA, with the addition of 5 QX-314 bromide, 5 TEA, 5 4-AP, 0.1 philanthotoxin, 1 MK-801, and 0.1% BSA. To isolate spontaneous or mini IPSCs in Purkinje cells, the internal solution contained the following (in mM): 100 CsCl, 10 EGTA, 10 HEPES, and 3 $MgCl_2$, pH 7.3 with CsOH. When perfusing a change in bath $[Ca]_o$, the $[Mg]_o$ was adjusted to yield a total divalent cation concentration of 3 mM. Except where noted, all recordings were performed in synaptic blockers that were bath applied after obtaining the initial seal: picrotoxin (50 μM), DL-2-amino-5-phosphonopentanoic acid (DL-AP5; 25 μM), 6,7-dinitroquinoxolinedione (DNQX; 10 μM; Tocris Cookson), and (2*S*)-3-([(15)-1-(3,4-dichlorophenyl)ethyl]amino-2-hydroxypropyl)(phenylmethyl) phosphinic acid (CGP55845; 1 μM; Tocris Bioscience). 2-Methyl-6-(phenylethynyl)pyridine hydrochloride (MPEP) (1 μM), (3,4-Dihydro-2H-pyrano[2,2-b]quinolin-7-yl)-(cis-4-methoxycyclohexyl)-methanone (JNJ-16259685) (1.5 μM), and AM-251 (2.5 μM) were used where indicated. Mouse monoclonal antibodies directed at either KChIP1 or KChIP3 isoforms (NeuroMab) were included in the internal electrolyte at 1:100 dilution.

Electrophysiology. Neuronal current- and voltage-clamp recordings were performed at 33–35°C and tsA-201 cell recordings at 21°C using a Multiclamp 700B amplifier and pClamp 10.1 software (Molecular Devices). Borosilicate pipettes (1.5 mm outer diameter) had a resistance of 6–8 MΩ with access resistance 8–15 MΩ (80–90% compensation in voltage clamp). Cells were rejected if access resistance drifted by >20%. Climbing fibers were stimulated with a monopolar stimulating electrode placed in the granule cell layer. A calculated junction potential of −10.7 mV in current-clamp recordings was subtracted from all data, while a negligible junction potential for voltage-clamp recordings was not subtracted. For on-cell recordings of Purkinje cell firing frequency, the pipette was held at a command potential of −40 mV to promote spontaneous spike discharge.

Dynamic Clamp. Dynamic-clamp recordings used a National Instruments BNC-2090 Digital/Analog converter and a computer running 64-bit OpenSuSE 11.1 with a real-time kernel. Real-time Experimental Interface (Dorval et al., 2001) was used for data recording and real-time calculations of injected conductances using voltage samples collected at 40 kHz. A measured junction potential of −10.7 mV was subtracted from all recordings and taken into account for conductance calculations. Custom scripts were used to simulate K_v4 currents. To adjust the biophysical properties of the K_v4 current under control and low $[Ca]_o$ conditions, two K_v4 currents were jointly simulated using the Hodgkin–Huxley formulism, and current calculations were made based on somatic voltage. The two currents differed only by their V_h of inactivation, which was determined using the following equation:

$$V_h = \frac{(-81.12 + 67.96)}{1 + e^{\frac{[ca]_o - 1.12}{0.098}}} - 67.96$$

where $[Ca]_o$ is extracellular calcium concentration in mM.

One of the K_v4 currents ($I_{K,\,exp}$) had a V_h of inactivation corresponding to the experimental $[Ca]_o$, while the other current ($I_{K,\,model}$) had a V_h determined by a hypothetical $[Ca]_o$. The difference between $I_{K,\,exp}$ and $I_{K,\,model}$ represented the change in I_K due to changes in calcium and corresponding physiological shifts in V_h. The difference current was injected at the somatic level, adjusting the biophysical parameters of the neuronal current online. To ensure the conductance density was within a physiological range, cell capacitance was first measured and then used to estimate cell surface area. This area was then multiplied by 42.6 pA/pF, the average conductance density of K_v4 channels in stellate cells. Conductance density was then adjusted to within 10% of this estimate.

Spike threshold was detected using a custom Matlab script by conducting a first derivative analysis of the voltage record to identify the absolute voltage at which instantaneous velocity was 3 SDs greater than the velocity of baseline voltage changes.

Paired recordings. For paired recordings, simultaneous whole-cell recordings were obtained under current clamp from stellate cells and voltage clamp from the soma of Purkinje cells, respectively. Cell pairs were obtained by first securing a whole-cell recording from a Purkinje cell and then a stellate cell contained within the expected span of the Purkinje cell dendritic arbor in the molecular layer directly above. In some cases stellate cells immediately adjacent to the recorded Purkinje cell were verified through direct visualization using differential interference contrast optics. Stellate cells were held just below threshold at rest and spike output evoked using 1 s current pulses, while Purkinje cells were maintained at a holding potential of −65 mV to record IPSCs. In all paired recordings, excitatory synaptic transmission was blocked by bath-applied DL-AP5 (25 μM) and DNQX (10 μM) and inhibitory transmission by bath applied CGP55845 (1 μM).

Spike-triggered averages (STAs) were calculated off-line in Matlab by time stamping the occurrence of stellate cell spikes and reverse correlating a period of 50 ms following the spike in the Purkinje cell record to extract postsynaptic events, with all events averaged in relation to presynaptic spike times. Failures were identified visually and were defined by

a lack of a sharp, well-defined inward current of at least 5 pA within 5 ms of the spike peak.

Charge transfer for spontaneous IPSCs was determined by dividing each trace into sections (1 s) and summing the charge transferred for currents greater than one SD (of the control condition) above baseline. To compensate for long-term drift in the recordings, the mean was subtracted from each time section before analysis was performed. To calculate the charge transfer of single stellate cell IPSCs under different conditions, STAs were taken from dual recordings of connected stellate and Purkinje cells. STAs from each condition were fit with the sum of two exponentials of the form $y = Ae^{-t/\tau_{rise}} + Be^{-t/\tau_{decay}}$. For 1.5 mM $[Ca]_o$, $A = 95$ pA, $B = -85$ pA, $\tau_{rise} = 0.4$ ms, and $\tau_{decay} = 11$ ms. For 1.1 mM $[Ca]_o$, $A = 40$ pA, $B = -37$ pA, $\tau_{rise} = 0.4$ ms, and $\tau_{decay} = 9$ ms.

Data and statistical analyses. Voltage-clamp analysis using Origin 8.0 (OriginLab) consisted of fitting steady-state inactivation curves with Boltzmann functions of the following form:

$$Y = \frac{A1 - A2}{1 + e^{\frac{x - xo}{dx}}} + A2$$

Dose–response relationships were fit with the following Hill equation:

$$y = \frac{[x]^N}{k^N + [x]^N}$$

Spontaneous IPSC (sIPSC) frequency and amplitudes were measured using a custom Matlab program. Current traces were filtered and local minima and maxima were identified. A local current deviation was determined to be a synaptic event if the difference between the minima and maxima was more than two times the SD of the current trace recorded in picrotoxin, which is assumed to represent the underlying noise. The velocity of the current deviation also had to exceed 0.1 pA/ms, a value determined to reliably identify IPSCs based on visual inspection. This method likely underestimates the frequency of sIPSCs and is sensitive to changes in the parameters (amplitude and velocity threshold). However, the ratio of frequencies and amplitudes among all three conditions was consistent for all sets of parameters.

Average values are indicated as mean ± SEM. Unless noted otherwise, all statistical tests were paired *t*-tests or one-way ANOVA with *post hoc* Tukey's HSD test.

Results

The Ca_v3–K_v4 complex is modulated by a range of $[Ca]_o$

Measurements of $[Ca]_o$ in the cerebellar molecular layer *in vivo* have revealed a decrease in $[Ca]_o$ from 1.2 mM to as low as 0.8 mM during 5 Hz climbing fiber stimulation (Stöckle and ten Bruggencate, 1978). We showed previously that blocking Ca_v3 calcium current causes a hyperpolarizing shift in the half-inactivation voltage (V_h) of stellate cell I_A, effectively reducing the availability of I_A (Anderson et al., 2010b). However, the ability for the Ca_v3–K_v4 complex to respond to the shifts in $[Ca]_o$ that occur during physiological rates of activity is unknown.

We measured the effects of bath perfusing various concentrations of $[Ca]_o$ (0.1–2.2 mM) on the inactivation voltage of I_A in stellate cells. I_A was isolated pharmacologically by blocking sodium, hyperpolarization-activated cyclic nucleotide-gated cation (HCN), and noninactivating potassium currents through bath application of 100 nM TTX, 2 mM Cs^+, and 5 mM TEA, respectively. Calcium channel blockers were specifically excluded to allow low voltage-activated Ca_v3-mediated calcium influx (I_T) during voltage commands. Under these conditions, the primary current recorded is a LVA, fast inactivating I_A (Fig. 1*A*). The V_h of I_A was determined using 1 s conditioning steps from −110 to 0 mV in 10 mV steps followed by a test pulse to −30 mV. A test pulse of −30 mV was used, as it corresponds to the peak of I_T activation and is within the range of I_A activation, but below that of high voltage-activated (HVA) calcium currents. In this regard, previous work has shown that stellate cells exhibit little HVA calcium current (Anderson et al., 2010b), and that none of the HVA calcium channels modulate the K_v4–KChIP3 interaction even when overexpressed in a heterologous system (Anderson et al., 2010b).

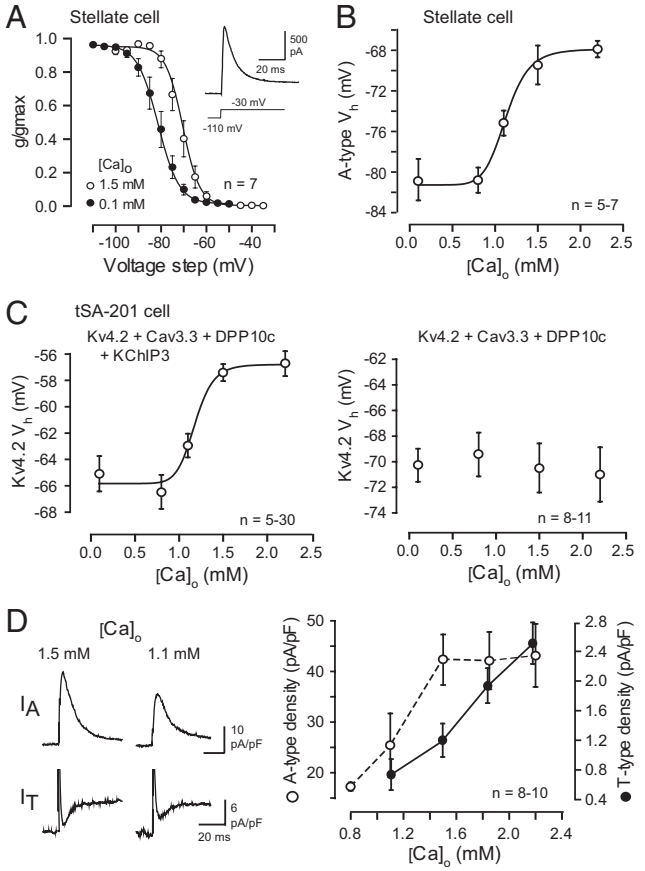

Figure 1. A physiologically relevant decrease of $[Ca]_o$ shifts the V_h of I_A. ***A***, Inactivation plots of stellate cell I_A recorded in 1.5 or 0.1 mM $[Ca]_o$ from a holding potential of −110 mV, followed by a series of preconditioning voltages of 10 mV steps to 0 mV, and current amplitude tested with a test pulse to −30 mV (see inset). ***B***, The dose–response curve of the relationship between $[Ca]_o$ and mean I_A V_h in stellate cells. Voltage commands are as in ***A***. ***C***, Dose–response curve between $[Ca]_o$ and $K_v4.2$ V_h expressed in tsA-201 cells for a Ca_v3–K_v4 complex in the presence or absence of expressed KChIP3 protein. Voltage commands are as in ***A***. ***D***, The effects of varying $[Ca]_o$ on the density of I_A and I_T in two different stellate cells. I_A was first evoked by a step from −80 to −45 mV in 1.5 or 1.1 mM $[Ca]_o$, and I_T was then isolated in the same cells by perfusion of 20 mM 4-AP. On the right are plots of the mean densities of I_A and I_T as a function of $[Ca]_o$. Current densities are averages of 10 traces and normalized to membrane capacitance.

Under control conditions of 1.5 mM $[Ca]_o$, stellate cells exhibit an I_A with a V_h of −69.5 ± 1.9 mV ($n = 7$). Decreasing bath $[Ca]_o$ to 0.1 mM resulted in an approximately −10 mV hyperpolarizing shift in V_h for I_A to −80.8 ± 2.0 mV ($n = 7$) (Fig. 1*A*). In contrast, increasing $[Ca]_o$ to 2.2 mM did not shift the V_h of I_A (Fig. 1*B*; $n = 5$, $p > 0.05$, unpaired *t*-test), indicating that the V_h recorded under control conditions could not be further shifted in the depolarizing direction by increasing calcium conductance. As $[Ca]_o$ was decreased to levels between 1.5 and 0.1 mM $[Ca]_o$, the V_h exhibited a graded leftward hyperpolarizing shift, reaching a stable saturation point of −80.1 ± 1.2 mV at ~0.8 mM $[Ca]_o$ ($n = 5$, $p < 0.001$; Fig. 1*B*). The relationship between V_h and $[Ca]_o$ was readily fit with the Hill equation ($k = 1.1 \pm 0.1$ mM; Hill coefficient, $N = 8.3 \pm 2.4$) with a midpoint of −75.3 ± 1.3 mV at 1.1 mM $[Ca]_o$ ($n = 6$, $p < 0.05$; Fig. 1*B*). The effects of low $[Ca]_o$ on I_A availability were not due to a change in divalent charge screening,

as changes in $[Ca]_o$ were always offset by a corresponding change in $[Mg]_o$ to yield a total divalent cation concentration of 3 mM. We further confirmed that the mean V_h of I_A in stellate cells was not significantly different in 1.1 mM $[Ca]_o$ if $[Mg]_o$ was not elevated ($n = 5$, $p > 0.05$, unpaired t-test; data not shown), and that elevating $[Mg]_o$ by 0.4 mM did not affect $Ca_v3.3$ calcium current measured in tsA-201 cells ($n = 7$; data not shown). The effects of decreasing $[Ca]_o$ on K_v4 V_h are thus interpreted as a decrease of calcium influx through Ca_v3 T-type calcium channels.

To further examine the relationship between $[Ca]_o$ and the Ca_v3–K_v4 interaction, we recorded $K_v4.2$ current in tsA-201 cells coexpressing cDNA for $Ca_v3.3$, $K_v4.2$, KChIP3, and DPP10c as a representative complement of the Ca_v3–K_v4 complex in stellate cells (Anderson et al., 2010b). tsA-201 cells were bathed in an external medium containing 1.5 mM $[Ca]_o$ at rest. Under these conditions, the $K_v4.2$ V_h was -57.4 ± 0.6 mV ($n = 30$), a baseline value lower than that encountered in stellate cells, but not unexpected for differences in absolute voltage dependence when comparing cDNA expressed in a heterologous system. Importantly, varying $[Ca]_o$ between 0.1 and 2.2 mM again shifted the voltage dependence of K_v4 inactivation over a range of ~10 mV, similar to that found in stellate cells (Fig. 1*C*). $K_v4.2$ V_h reached a maximum hyperpolarized value of -66.5 ± 1.3 mV ($n = 6$) for a $[Ca]_o$ of 0.8 mM, with a V_h of -62.9 ± 0.9 mV at 1.1 mM $[Ca]_o$ ($n = 5$; $k = 1.2 \pm 0.1$ mM; $N = 11.2 \pm 5.4$). Importantly, the Ca_v3–K_v4 interaction has been shown to depend on KChIP3, an accessory calcium-sensing protein of the K_v4 complex (Anderson et al., 2010b). When cDNA encoding for KChIP3 proteins was omitted from the transfection medium, the dose–response relationship between $[Ca]_o$ and $K_v4.2$ V_h was abolished, with $K_v4.2$ V_h remaining stable at approximately −70 mV for all values of $[Ca]_o$ (Fig. 1*C*).

These data indicate that the effects of a decrease in $[Ca]_o$ on I_A availability derives at least in part from an interaction between I_T and KChIP3. Our understanding of the interaction between Ca_v3 and K_v4 channels suggests that the dose-dependent response of K_v4 V_h to $[Ca]_o$ reflects a shift in V_h due to a calcium-dependent KChIP3 interaction. The prediction is that K_v4 current density should plateau once all KChIP3 proteins are maximally bound as calcium influx increases with $[Ca]_o$. To test this we measured the peak density of I_A and I_T under different $[Ca]_o$ (Fig. 1*D*). I_A density was assessed with I_T left intact, and then I_T was isolated in the same cell by bath application of 4-AP (20 mM) and evoked using the same step command (Fig. 1*D*). Control tests established that 20 mM 4-AP has no effect on the current–voltage relationship of either $Ca_v3.2$ or $Ca_v3.3$ channels, the two Ca_v3 channel isoforms expressed by stellate cells ($n = 6$; data not shown) (Molineux et al., 2006). While I_A could be recorded over a range of 0.8–2.2 mM $[Ca]_o$, I_T could not be reliably resolved below 1.1 mM $[Ca]_o$, restricting I_T density measurements to 1.1–2.2 mM $[Ca]_o$. These tests showed that I_T peak density exhibited a linear increase over the full range of 1.1 to 2.2 mM $[Ca]_o$, as predicted by an increased driving force and the number of permeant ions as $[Ca]_o$ was raised. In contrast, I_A peak density followed the shift in V_h established for different levels of $[Ca]_o$ in Figure 1*B*, reaching a plateau of maximal density for $[Ca]_o$ levels of 1.5 mM or greater (Fig. 1*D*).

These data establish that K_v4 availability can be modulated within the range of shifts in $[Ca]_o$ that have been reported to occur under physiological conditions *in vivo*. The results also indicate that reductions in $[Ca]_o$ will decrease Ca_v3-mediated calcium influx and reduce the availability of K_v4 current in a manner consistent with an action through the Ca_v3–K_v4 complex.

Climbing fiber input decreases stellate cell I_T and I_A

To be physiologically relevant, the low calcium-induced change in K_v4 availability should be reproduced by direct activation of synaptic inputs in the molecular layer. In this regard, climbing fibers present an especially interesting case for potential regulation of the Ca_v3–K_v4 complex. Climbing fiber boutons have been shown to overlap with the soma and dendritic processes of stellate cells (Nishiyama et al., 2007; Brown et al., 2012), while ultrastructural analyses reveal boutons that are tightly apposed to stellate cell membranes, but without evidence for vesicular release machinery (Hámori and Szentágothai, 1980; Kollo et al., 2006). In fact, the locations at which climbing fiber boutons align with stellate cells closely matches the distribution pattern of K_v4 channel immunolabel in stellate cell membranes, a highly unusual relationship for which there was no known function (Kollo et al., 2006). Although the distribution of Ca_v3 channels has not been determined at the ultrastructural level, the known association between Ca_v3 and K_v4 channels within a functional nanodomain (<50 nm) (Anderson et al., 2010b) suggests that Ca_v3 channels will be found in close proximity to some number of the K_v4 channels at these junctions. Climbing fiber activation is further interesting in reportedly generating a reduction in $[Ca]_o$ (Stöckle and ten Bruggencate, 1980) in the course of generating a calcium-dependent complex spike in Purkinje cells that conducts throughout the dendritic tree (Llinás and Sugimori, 1980b; Kitamura and Häusser, 2011), where stellate cells are embedded.

Sensing changes in calcium driving force

We wished to test whether repetitive climbing fiber stimulation could evoke a decrease in $[Ca]_o$ that in turn alters the availability of I_A through the Ca_v3–K_v4 interaction. To date, the only measure of a change in $[Ca]_o$ during climbing fiber stimulation was obtained using calcium-selective microelectrodes *in vivo* (Heinemann et al., 1977; Nicholson et al., 1978; Stöckle and ten Bruggencate, 1980; McCreery and Agnew, 1983). The ability to evoke a decrease in $[Ca]_o$ *in vitro* during repetitive synaptic input must also contend with the technical necessity of perfusing a fixed level of calcium in the bathing medium. We note, however, that the recordings of I_T in stellate cells in Figure 1*D* indicate that a change in $[Ca]_o$ in the bathing medium can be detected as a change in driving force, as reflected by a linear reduction in I_T density as $[Ca]_o$ is lowered, with an ~30% decrease in I_T when $[Ca]_o$ was lowered from 1.5 to 1.1 mM. We thus tested whether repetitive climbing fiber stimulation could decrease I_T in a manner consistent with a change in the driving force for calcium. In this way we could effectively use the stellate cell itself as a delicate sensor for any changes in $[Ca]_o$ in the surrounding microenvironment during *in vitro* recording conditions.

To examine the effect of climbing fiber stimulation on I_T in stellate cells, we simultaneously recorded from the soma of a Purkinje cell and that of a stellate cell visualized directly above in the molecular layer, and thus presumably within or near the dendritic arbor of the recorded Purkinje cell. In some cases this could be confirmed by tracking the course of a Purkinje cell dendritic tree through DIC-IR optics to the position of the targeted stellate cell. We then stimulated climbing fiber input to simultaneously monitor complex spike discharge in the Purkinje cell and I_T in the stellate cell. I_T was isolated by including in the electrode 5 mM QX-314 to block sodium channels and 5 mM 4-AP and 5 mM TEA to block I_A and any delayed rectifying potassium channels. Although internal QX-314 can affect some calcium currents (Talbot and Sayer, 1996), we confirmed that we could record I_T with a stable baseline amplitude of 8.4 ± 1.9 pA ($n = 6$; maxi-

mum 20 pA) that reliably recovered to control levels following trains of synaptic stimulation. Blockade of any remaining potassium channels was ensured by using a CsCl-based internal electrolyte. Synaptic activation of stellate cells (Jörntell and Ekerot, 2003; Szapiro and Barbour, 2007; Barmack and Yakhnitsa, 2008) was blocked by internal perfusion of 100 μM philanthotoxin to block AMPA receptors (Nilsen and England, 2007) and 1 mM MK-801 to block NMDA receptors, and bath application of 1 μM MPEP, 1.5 μM JNJ-16295685, and 2.5 μM AM-251 to block potential activation of group I metabotropic glutamate or CB1 receptors (Gatley et al., 1996; Gasparini et al., 1999; Crepel and Daniel, 2007; Knöpfel, 2007). Under these conditions, the majority of synaptic currents were blocked with only occasional fast spontaneous synaptic currents in four of six cells (mean of -57.8 ± 20.0 pA amplitude; $n = 4$). Spontaneous synaptic events were not associated with climbing fiber stimulation and were readily distinguishable from I_T, but any records with overlapping spontaneous synaptic currents were discarded. In this way, I_T could be recorded in stellate cells while preserving climbing fiber-evoked complex spike discharge in nearby Purkinje cells.

Voltage pulses were delivered to stellate cells from a holding potential of -110 to -45 mV (50 ms) at a 5 Hz base rate (Fig. 2*A*) to measure I_T near its peak voltage on *I–V* plots. After 2.5 s of control recording, a climbing fiber stimulus was interleaved with step commands by stimulating at 10 Hz (10 pulses), and recordings of I_T continued for at least 5 s after stimulation was terminated. Data from recordings were accepted when I_T density was sufficient to evoke a clearly resolved transient inward current, a complex spike was reliably evoked in the Purkinje cell, and recovery of I_T peak amplitude was apparent after synaptic stimulation. I_T peak amplitude was stable during control pulses, but declined rapidly during climbing fiber stimuli (Fig. 2*A*), reducing from an original peak value of 8.4 ± 1.9 pA to 5.5 ± 1.8 pA ($n = 6$) by the end of the 10 pulse stimulus train, reflecting a $42.2 \pm 11.8\%$ decrease in amplitude ($n = 6$, $p < 0.05$, one-way repeated measures ANOVA, Tukey's pairwise comparison). Within 1 s following a stimulus train, I_T peak amplitude had recovered to 8.2 ± 1.5 pA ($n = 6$, $p = 0.98$), a level that was not significantly different from control. Full recovery was apparent by 5 s (8.45 ± 1.92 pA, $n = 6$).

A reduction in I_T density could come about through a change in Ca_v3 channel insertion in the membrane, a reduction in conductance through the action of a ligand or a shift in voltage-dependent properties, or a reduction in calcium driving force. It seems highly unlikely that the density of Ca_v3 channels in the plasma membrane could be reduced and restored to control levels within ~1 s time in relation to climbing fiber stimulation. We note that we cannot fully exclude the possibility that an unknown ligand (such as that producing occasional spontaneous synaptic events observed in stellate cells under our conditions) could have affected Ca_v3 channel conductance, although we did not detect any synaptic responses evoked by climbing fiber stimuli per se. We also have no evidence to support a shift in the voltage dependence of Ca_v3 channels, a parameter that would be difficult to test in the short time frame associated with changes in I_T density recorded here. Rather, the results presented in Figure 1*D* indicate that even subtle decreases in $[Ca]_o$ are sufficient to substantially alter I_T density, and in a linear fashion as predicted for a shift in calcium driving force. In fact, comparing the 40% mean reduction in I_T density recorded during climbing fiber stimulation (Fig. 2*D*) to that recorded during bath perfusion of different levels of $[Ca]_o$ predicts a potential climbing fiber-induced change in $[Ca]_o$ of 0.63 mM (from 1.5 mM down to 0.87 mM). These data

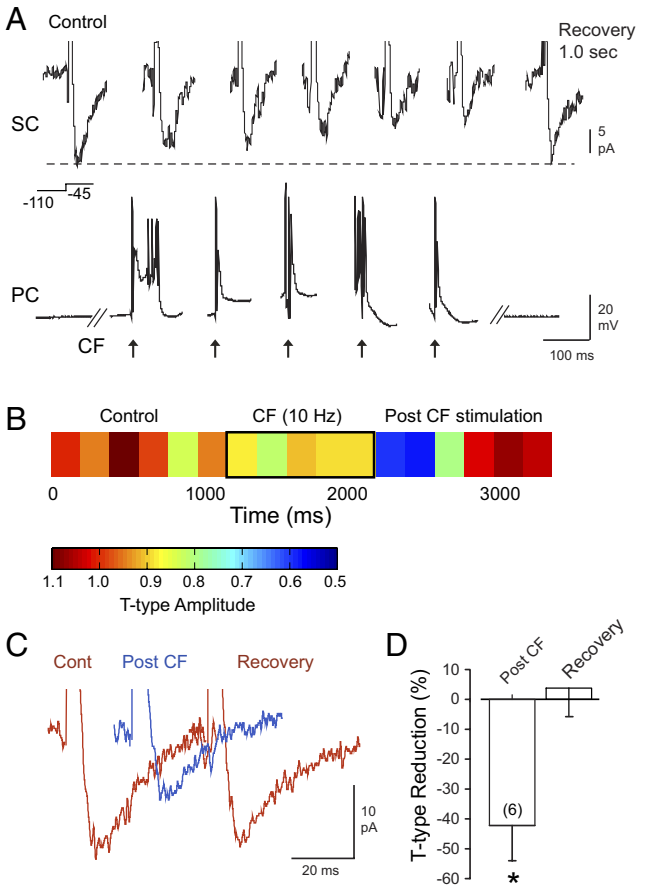

Figure 2. Repetitive 10 Hz climbing fiber stimulation evokes a decrease in stellate cell I_T. ***A***, Dual recordings of I_T in a stellate cell (SC) and spike discharge in a Purkinje cell (PC) soma recorded in the cell layer directly below the SC. Synaptic responses are pharmacologically blocked in the SC to allow activation of complex spikes in the Purkinje cell by climbing fiber (CF; arrows) stimulation. I_T is evoked by a step from -110 to -45 mV (5 Hz), and CF stimuli are interleaved with the step commands using a 10 pulse 10 Hz CF stimulus. Recordings are shown for control (left), every second CF stimulus during the 10 pulse train (middle), and 1.0 s after the end of the train (Recovery; right). The dashed line below recordings marks the control I_T amplitude for comparison. ***B***, Mean values for I_T amplitude normalized and color coded with respect to the mean of control pulses preceding CF stimulation ($n = 6$). The period of 10 Hz CF stimulation is shown bounded by a box. ***C***, Expanded and superimposed representative records of I_T in control, immediately post CF stimulation, and recovery 1.0 s after the stimulus train, as for experiments in ***A*** and ***B***. ***D***, Bar plots of the mean change in I_T amplitude immediately following CF stimulation (Post CF) and 1.0 s following the end of the stimulus train. For display purposes, stimulus and capacitative artifacts are digitally reduced in ***A*** and ***C*** and a slight shift in baseline inward current during CF stimulation is removed from I_T recordings in ***A***. Sample values are shown in brackets within the bar plot. *$p < 0.05$.

are important in revealing that climbing fiber stimulation reduces I_T in a manner consistent with a decrease in $[Ca]_o$ in the microenvironment surrounding stellate cells even under *in vitro* recording conditions.

Stimulus-evoked reductions in I_A

We next repeated these tests to examine the effect of repetitive climbing fiber stimulation on the amplitude of I_A in stellate cells. We thus obtained dual recordings from the soma of a Purkinje cell and a stellate cell positioned directly above in the molecular layer. I_A was isolated in stellate cells by including 5 mM QX-314 and 5 mM TEA in the electrode using a KCl-based internal electrolyte, and complex spike discharge was recorded in the Purkinje cell in current-clamp

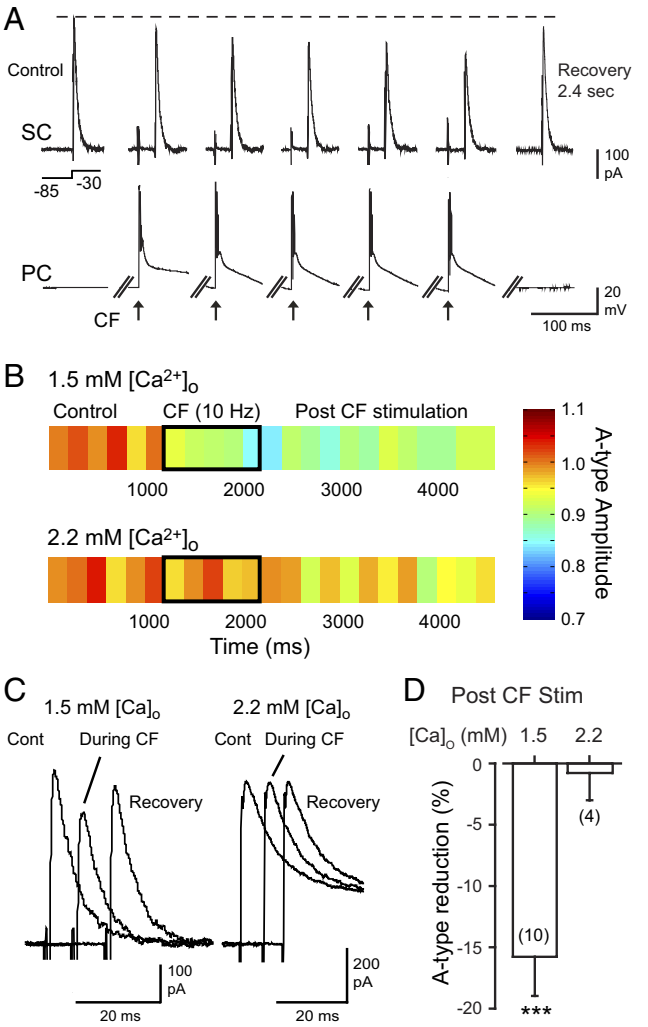

Figure 3. Repetitive 10 Hz climbing fiber stimulation evokes a decrease in stellate cell I_A. ***A***, Dual recordings of I_A in a stellate cell (SC) and spike discharge in a Purkinje cell (PC) soma recorded in the cell layer directly below. Synaptic responses are pharmacologically blocked in the SC to allow selective activation of complex spikes in the Purkinje cell through climbing fiber (CF; arrows) stimulation. I_A is evoked by a step from −85 to −30 mV (5 Hz), and CF stimuli are interleaved with the step commands using a 10 pulse, 10 Hz CF stimulus. Recordings are shown for control (left), every second CF stimulus during the 10 pulse train (middle), and after 2.4 s recovery (right). The dashed line above recordings marks the control I_A amplitude for comparison. ***B***, Mean values for I_A amplitude normalized and color coded with respect to the mean of six control pulses preceding CF stimulation when recorded in 1.5 mM $[Ca]_o$ ($n = 10$) or 2.2 mM $[Ca]_o$ ($n = 4$). The period of 10 Hz CF stimulation is shown bounded by a box. ***C***, Expanded and superimposed representative records of I_A in 1.5 or 2.2 mM $[Ca]_o$ in control, during CF stimulation, and recovery 2.4 s after the stimulus train, as for experiments in ***A*** and ***B***. ***D***, Bar plots of the mean change in I_A amplitude immediately following the CF stimulus train in 1.5 or 2.2 mM $[Ca]_o$. Note the rapid decrease in peak I_A during CF stimulation in 1.5 mM $[Ca]_o$ and the lack of effect in 2.2 mM $[Ca]_o$ to offset stimulus-induced changes in $[Ca]_o$. For display purposes, recordings are truncated in ***A***. Stimulus and capacitative artifacts were digitally reduced in ***A*** and ***C***. Sample values are shown in brackets within bar plots. $^{***}p < 0.001$.

mode (Fig. 3*A*). The same set of internal and external synaptic blockers were applied as for recordings of I_T. In a separate set of experiments, we verified that QX-314 had no significant effect on the magnitude of the shift in K_v4 V_h induced by perfusing 1.1 mM $[Ca]_o$ ($n = 6, p > 0.05$, unpaired *t*-test; data not shown). I_A was evoked by a voltage step from −85 to −30 mV (50 ms) at a 5 Hz base rate to test I_A over the voltage range relevant to a shift in inactivation voltage. Control recordings of I_A were obtained over 1.5 s before interleaving a 10 Hz climbing fiber stimulus at 10 Hz (10 pulses). I_A peak amplitude was stable during the control pulses, but showed a progressive decrease during climbing fiber evoked complex spike discharge in a nearby Purkinje cell, reaching an average 15.8 ± 3.2% reduction after 10 stimuli (maximum 30%; $n = 10$, $p < 0.001$; Fig. 3*A*,*B*). At the end of the climbing fiber stimulus train, I_A amplitude gradually recovered, returning to 92.3 ± 1.6% of its original value by 2.4 s ($n = 10$, $p < 0.01$), and was fully recovered at 5 s to 1.0 ± 0.02 of control ($n = 8$, $p > 0.05$; Fig. 3*A*–*C*). Moreover, the reduction in I_A could be evoked in a reversible manner on repeated occasions at 5 min intervals, ruling out any significant washout over time.

Based on the V_h $[Ca]_o$ dose–response curve (Fig. 1*B*), we predicted that conducting these tests in 2.2 mM $[Ca]_o$ should prevent significant V_h shifts by offsetting any reduction in $[Ca]_o$ during climbing fiber stimulation. Therefore, in a subset of cells, we subsequently bath applied 2.2 mM $[Ca]_o$ ($n = 4$ of 10) for 5 min and retested the effects of climbing fiber stimulation on I_A amplitude. No significant decrease in I_A was detected in the presence of 2.2 mM $[Ca]_o$ (0.8 ± 2.2% decrease, $n = 4, p = 0.95$; Fig. 3*B*–*D*), even though the preceding trains in this group of cells decreased I_A by 10.6 ± 2.9% when delivered in 1.5 mM $[Ca]_o$ ($n = 4, p < 0.05$).

Collectively, these results are consistent with the interpretation that repetitive stimulation of complex spike discharge in Purkinje cells promotes a decrease in the driving force of Ca_v3-mediated calcium influx, which is accompanied by a reduction in the availability of I_A in stellate cells, as predicted for actions of the Ca_v3–K_v4 complex.

Physiological changes in $[Ca]_o$ alter stellate cell excitability

Outward current generated by I_A is capable of controlling several aspects of spike output, including spike latency, threshold, and frequency (Connor and Stevens, 1971a, b; Hoffman et al., 1997; Molineux et al., 2005; Khaliq and Bean, 2008; Anderson et al., 2010b; Norris and Nerbonne, 2010; Norris et al., 2010; Carrasquillo et al., 2012). We next examined the effect of decreasing $[Ca]_o$ from a resting level of 1.5 to 1.1 mM on firing frequency using on-cell recordings to avoid cell dialysis inherent to whole-cell recordings. Stellate cells exhibited a resting level of spontaneous discharge between 5 and 10 Hz (6.6 ± 0.5 Hz, $n = 35$) in 1.5 mM $[Ca]_o$. Decreasing $[Ca]_o$ to 1.1 mM resulted in a nearly two-fold increase in the rate of spontaneous discharge ($n = 6$) that was reversible when $[Ca]_o$ was returned to 1.5 mM (Fig. 4*A*). It is possible that the observed elevation in firing frequency in 1.1 mM $[Ca]_o$ could involve a decreased activation of calcium-dependent potassium channels. However, neither the SK channel blocker apamin (100 nM, $n = 6$, $p > 0.05$) nor the BK channel blocker paxilline (100 nM, $n = 5$, $p > 0.05$) affected the rate of spontaneous on-cell firing frequency.

A second issue to consider is that repetitive activation of synaptic inputs also elevates the extracellular concentration of potassium ($[K]_o$). In the molecular layer, 5 Hz climbing fiber discharge evoked by peripheral nerve stimulation *in vivo* produces an increase in $[K]_o$ of ~0.7 mM from resting conditions that could affect E_K and the driving force for I_A (Bruggencate et al., 1976; Stöckle and ten Bruggencate, 1980). However, we found that a 0.75 mM elevation of $[K]_o$ did not significantly alter either the rate of on-cell spike discharge ($n = 6, p > 0.05$) or the amplitude of I_A ($n = 10, p > 0.05$). A combined change in $[Ca]_o$ and $[K]_o$ reduced I_A amplitude ($n = 6$, $p < 0.05$), but it was not significantly different from that of 1.1 mM $[Ca]_o$ alone ($n = 6$, $p > 0.05$). These tests reveal that the increases in $[K]_o$ reported during physiological levels of climbing fiber stimulation *in vivo* are not sufficient to account for the effects detected here for associated decreases in

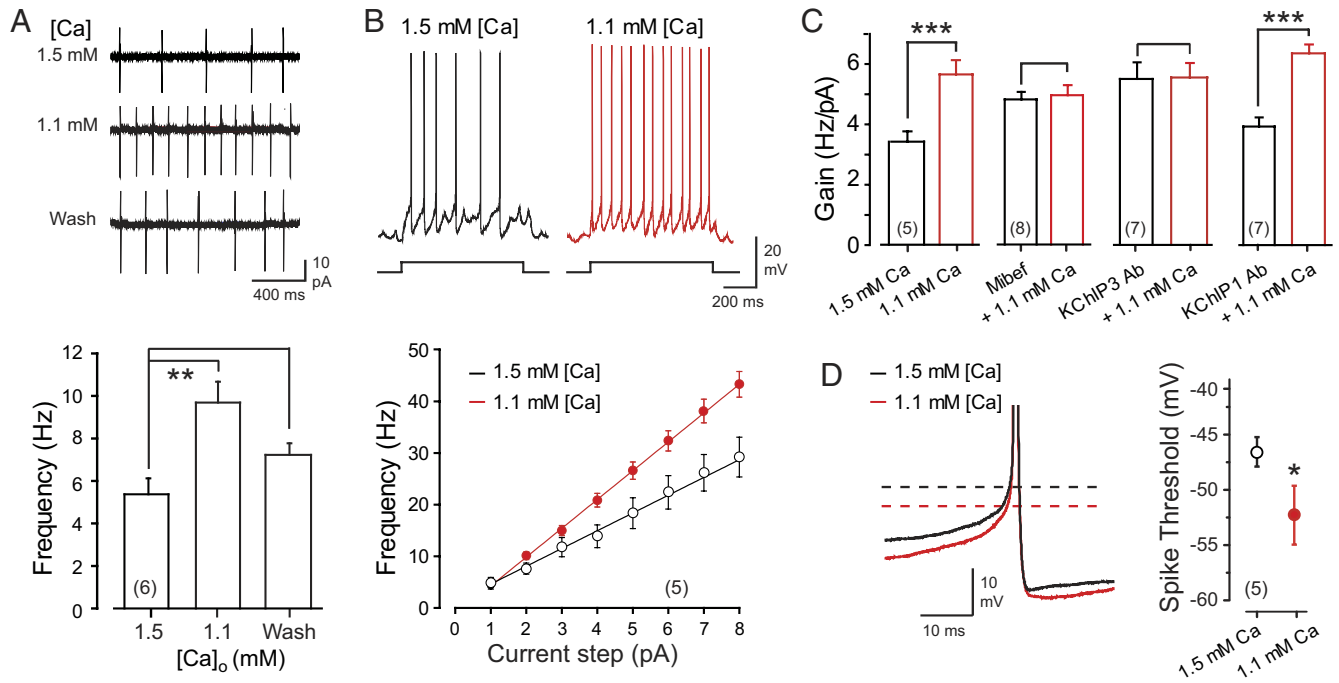

Figure 4. Low $[Ca]_o$ increases the gain and lowers the threshold of stellate cell firing. ***A***, ***B***, Lowering $[Ca]_o$ from 1.5 to 1.1 mM significantly increases the frequency of spontaneous stellate cell spike discharge in on-cell recordings and gain of intracellular spike discharge evoked by square wave current pulses to calculate current–frequency plots in ***B***. ***C***, Bar plots of the effect of 1.1 mM $[Ca]_o$ on gain of firing and its occlusion by pretreatment with mibefradil (Mibef; 500 nM) or infusion of an antibody against KChIP3 (1:100) through the patch electrode, but not by an antibody against KChIP1. ***D***, Recordings and scatter plot reveal a significant decrease in the absolute voltage threshold for spike discharge (dashed lines) in 1.1 mM $[Ca]_o$. Sample values are shown in brackets. $*p < 0.05$; $**p < 0.01$; $***p < 0.001$.

$[Ca]_o$. Therefore, we restricted further tests to changes in $[Ca]_o$ relevant to actual peripheral stimulation *in vivo*.

We showed previously that pharmacological blockade of Ca_v3 calcium channels and its interaction with the K_v4 channel complex increased the gain of firing in stellate cells (Anderson et al., 2010b). We next determined the effect of different levels of $[Ca]_o$ on stellate cell gain used whole-cell recordings. Applying a decrease in $[Ca]_o$ from 1.5 to 1.1 mM to reduce I_A availability revealed an ~65% increase in the gain of stellate cell firing on current–frequency plots ($n = 5$, $p < 0.001$; Fig. 4*B*,*C*). The increase in gain was not related to any secondary regulation of internal calcium stores, as the gain of stellate cell firing increased in a similar manner in the presence of internal heparin (4 mg/ml) and bath-applied 6 μM cyclopiazonic acid to block any IP3-mediated calcium release and calcium ATPases ($n = 8$, $p < 0.05$). Pretreating slices with the Ca_v3 channel blocker mibefradil (500 nM) further occluded the effects of 1.1 mM $[Ca]_o$ on the gain of firing frequency ($n = 8$), supporting the interpretation that the increase in gain is mediated by Ca_v3 calcium influx (Fig. 4*C*).

One means of interrupting the Ca_v3-KChIP3 interaction is by internally infusing a monoclonal KChIP3 antibody (Anderson et al., 2010b). We thus infused KChIP antibodies (1:100 dilution) through the electrode to test the ability for low $[Ca]_o$ to induce a change in the gain of firing. Frequency–current plots were constructed at 10 min intervals for up to 30 min following entry in the whole-cell configuration to allow full dialysis of KChIP antibodies. These tests revealed that infusion of a KChIP3 antibody occluded the ability of 1.1 mM $[Ca]_o$ to increase the gain of firing ($n = 7$; Fig. 4*C*). By comparison, infusion of a monoclonal antibody against KChIP1 (1:100 dilution), a protein not expressed in stellate cells, did not prevent an increase in gain of firing by 1.1 mM $[Ca]_o$ ($n = 7$, $p < 0.001$; Fig. 4*C*).

A closer examination of the process of spike firing revealed that the increase in gain of firing in 1.1 mM $[Ca]_o$ was associated with a significant decrease in spike threshold voltage, with the point of membrane potential transition to spike output shifting in a negative direction by 4–10 mV ($n = 5$, $p < 0.05$; Fig. 4*D*). The increase in spike frequency in low $[Ca]_o$ could also be accompanied by a decrease in the amplitude of the AHP, although the magnitude of these changes were variable and not statistically significant (data not shown). The loss of I_A and outward current during the interspike interval in low $[Ca]_o$ can thus reduce spike threshold, identifying one factor contributing to the increase in firing frequency.

The Ca_v3–K_v4 complex adjusts firing rate in response to fluctuations in $[Ca]_o$

To determine the extent to which a selective shift in the V_h of stellate cell I_A can alter the gain or threshold of stellate cell firing, we applied dynamic clamp. For this we used the established biophysical properties of I_A and I_T in stellate cells (Molineux et al., 2005), the dose–response relationship between $[Ca]_o$ and I_A V_h values (Fig. 1*B*), and the inactivation curves in 1.5 versus 1.1 mM $[Ca]_o$ to estimate the h_∞ values reflecting I_A availability. These data were then used to iteratively simulate either condition of $[Ca]_o$ and dynamically modulate the I_A available at each voltage sampled during a spike response (25 μs sampling interval). In this way, a cell could be maintained in either 1.5 or 1.1 mM $[Ca]_o$ and dynamic clamp used to simulate a shift in I_A availability typical of a change in $[Ca]_o$ without altering the driving force for calcium entry. Practically, this equated to calculating the I_A predicted to be available for either $[Ca]_o$ and then injecting or subtracting the difference current (Fig. 5). Simulating a shift from an actual level of 1.5 mM $[Ca]_o$ in the bath to a "virtual" 1.1 mM $[Ca]_o$ thus predicted a net inward current that acted in a depolarizing

manner during the time course of an evoked spike (Fig. 5*B*). Conversely, if a cell was held in 1.1 mM $[Ca]_o$, we simulated the condition relevant to I_A availability for a virtual increase of $[Ca]_o$ to 1.5 mM by injecting an outward difference current during the course of a spike (Fig. 5*C*). Thus, the availability of I_A that would be characteristic of a given $[Ca]_o$ could be applied on-line without directly manipulating $[Ca]_o$ or I_T.

The effects of dynamically modulating I_A availability are shown in Figure 6. Recordings were first performed in 1.5 mM $[Ca]_o$, and the gain of firing frequency measured using current pulses under conventional current clamp to construct a frequency–current plot. Subtraction of I_A using dynamic clamp to simulate a left shift in V_h relevant to 1.1 mM $[Ca]_o$ caused a substantial increase in gain of firing ($n = 6$, $p < 0.05$; Fig. 6*A*,*C*). We note that an additional increase in the initial rate of firing on the frequency–current plot was apparent for the dynamic clamp subtraction of I_A (Fig. 6*A*), likely reflecting the depolarizing action of I_T that remains intact under these conditions. Recordings from the same neurons were then performed in the presence of 1.1 mM $[Ca]_o$ in the bath to reduce the Ca_v3–K_v4 interaction and increase gain in the expected manner, as evident by an increased rate of firing and slope of the baseline frequency–current plot (Fig. 6*B*). Dynamic injection of I_A that would be expected in the presence of 1.5 mM $[Ca]_o$ then restored excitability by decreasing the gain of firing to within control levels ($n = 6$, $p < 0.05$; Fig. 6*B*,*C*). Consistent with results in bath-applied low $[Ca]_o$, a reduction of I_A via dynamic clamp for cells bathed in 1.5 mM $[Ca]_o$ also resulted in a significant decrease in spike threshold ($n = 6$, $p < 0.01$; Fig. 6*C*). Conversely, dynamic addition of I_A in cells perfused initially with 1.1 mM $[Ca]_o$ significantly increased spike threshold ($n = 6$, $p < 0.05$; Fig. 6*C*). Collectively, these results demonstrate that a selective shift in the V_h for I_A (without affecting calcium conductance directly) is sufficient to account for the changes in gain of stellate cell firing during fluctuations of $[Ca]_o$, again implicating a key role for the Ca_v3–K_v4 complex.

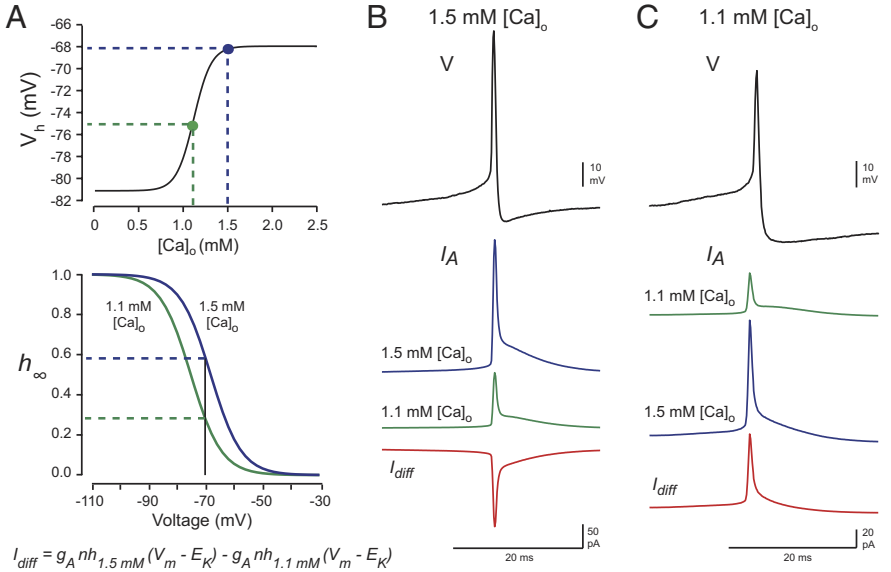

Figure 5. Simulating a selective shift in I_A voltage for inactivation through dynamic clamp. ***A***, The stellate cell I_A V_h $[Ca]_o$ dose–response curve (top) and shift in I_A h_∞ for 1.5 or 1.1 mM $[Ca]_o$ (bottom). The dashed lines (top) represent the calculated V_h for I_A in the presence of 1.5 mM $[Ca]_o$ (blue) or 1.1 mM $[Ca]_o$ (green; Fig. 1*B*). Fits of the mean inactivation curves of stellate cell I_A (bottom) for 1.5 and 1.1 mM $[Ca]_o$ are used to iteratively calculate the h_∞ values and difference currents for I_A (I_{diff}). Dashed lines indicate the h_∞ values calculated for either condition at −70 mV. I_{diff} is then added or subtracted to simulate conditions of 1.5 or 1.1 mM $[Ca]_o$ in real time during the spike (25 μs sampling interval). ***B***, ***C***, Recordings of single spike responses (top row) performed in the presence of 1.5 mM $[Ca]_o$ or 1.1 mM $[Ca]_o$, but modulated through dynamic clamp according to the predicted availability of I_A at the alternate $[Ca]_o$. The second row represents the I_A predicted for the $[Ca]_o$ indicated, the third row the I_A predicted to be available at the alternate $[Ca]_o$, and the fourth row the difference current calculated to dynamically add or subtract to simulate the alternate $[Ca^{2+}]_o$ condition. The I_{diff} was inward in ***B*** and had a depolarizing effect on membrane potential, and outward in ***C*** with a hyperpolarizing effect on membrane potential.

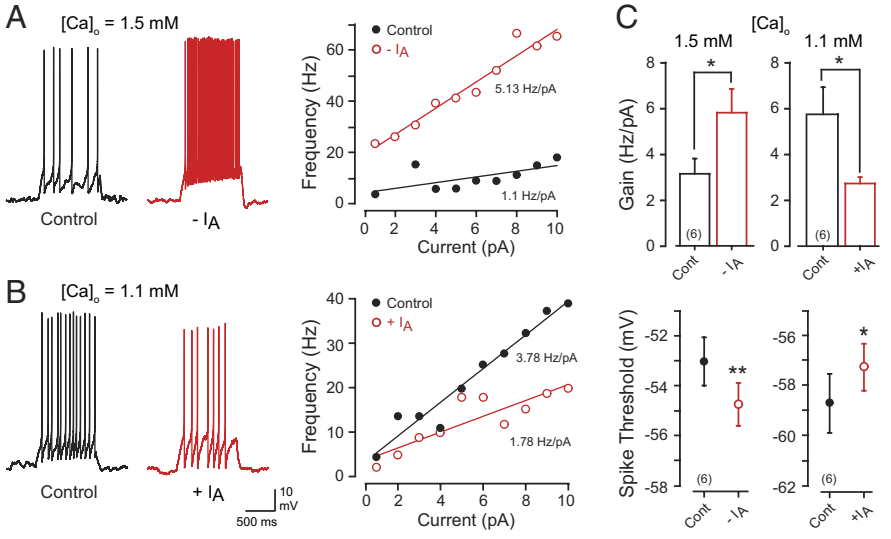

Figure 6. Dynamic subtraction or addition of I_A modulates the gain and threshold of stellate cell firing. ***A***, ***B***, A comparison of the effects of recording spike output in a stellate cell maintained in 1.5 mM $[Ca]_o$ and then subtracting I_A to simulate a shift to 1.1 mM $[Ca]_o$ (***A***), and the same cell now perfused with 1.1 mM $[Ca]_o$ before (black) and after dynamic clamp injection of I_A (red) according to the predicted availability of I_A in 1.5 mM $[Ca]_o$ (***B***). Representative traces of current-evoked spike output and the associated current–frequency plots are shown. ***C***, Plots of the average effect of either dynamically subtracting I_A in cells perfused with 1.5 mM $[Ca]_o$ (left column) or dynamically adding I_A to cells perfused in 1.1 mM $[Ca]_o$ (right column) on the gain of firing frequency and spike voltage threshold. Lines on current–frequency plots represent best-fit calculations to the data, and sample values are shown at the base of bar plots. *$p < 0.05$; **$p < 0.01$.

The Ca_v3–K_v4 complex maintains inhibitory synaptic efficacy during reductions of $[Ca]_o$

Synaptic transmission depends critically on calcium influx into presynaptic terminals to cause vesicle fusion and transmitter release. Any change in $[Ca]_o$ would then be expected to reduce release probability within the local environment. This is important, as a decrease in release probability could reduce the net inhibitory charge transferred to Purkinje cells when excitatory synaptic input lowers $[Ca]_o$. We thus tested the effects of low $[Ca]_o$ on synaptic transmission between stellate and Purkinje

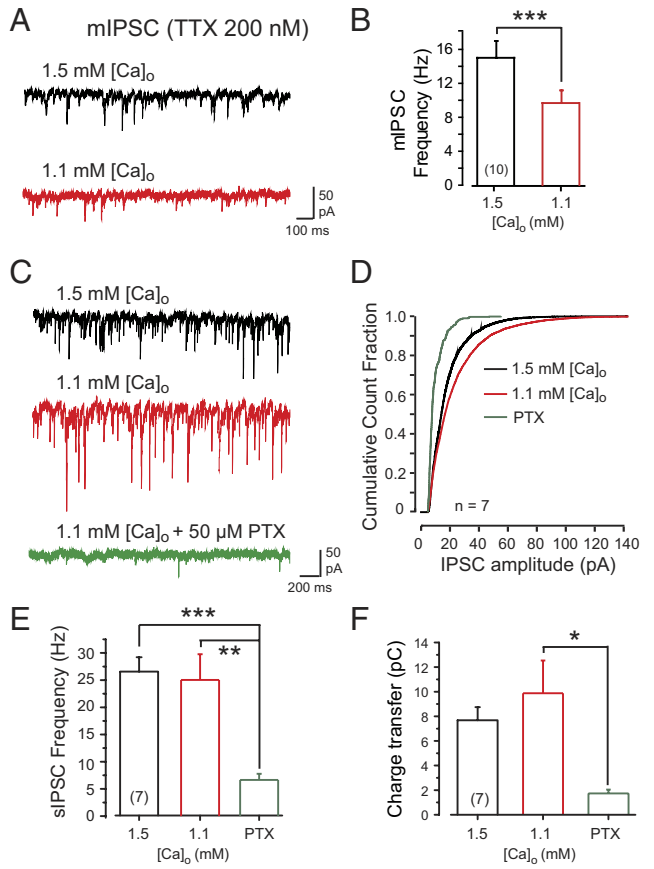

Figure 7. Inhibitory charge transfer of sIPSCs to Purkinje cells is maintained in low $[Ca]_o$. ***A***, mIPSCs recorded from a Purkinje cell in the presence of 200 nM TTX to block presynaptic spike discharge in 1.5 and 1.1 mM $[Ca]_o$. ***B***, Bar plots of average mIPSC frequency reveal a significant decrease in mIPSC frequency in low $[Ca]_o$. ***C***, sIPSCs recorded from a Purkinje cell in 1.5 mM $[Ca]_o$ and 1.1 mM $[Ca]_o$. The internal electrolyte was a CsCl-based solution, and DNQX and DL-AP5 were bath applied to block excitatory synaptic transmission. Lowering $[Ca]_o$ to 1.1 mM increases the amplitude of sIPSCs, while subsequent perfusion of the $GABA_A$ blocker picrotoxin (PTX; 50 μM) abolishes all sIPSCs. ***D***, A cumulative distribution function of sIPSC amplitudes indicating an increase in the proportion of large-amplitude sIPSCs with application of 1.1 mM $[Ca]_o$ compared to 1.5 mM $[Ca]_o$. ***E***, Mean bar plot of sIPSC frequency measured in 1.5 and 1.1 mM $[Ca]_o$ and after perfusion of picrotoxin indicate that sIPSC frequency is maintained in low $[Ca]_o$ and significantly decreases in the presence of picrotoxin. ***F***, Bar plots of the total charge transfer in Purkinje cell recordings in the presence of 1.5 or 1.1 mM $[Ca]_o$ and after perfusion of picrotoxin. Sample values are shown within bar plots. $*p < 0.05$; $**p < 0.01$; $***p < 0.001$.

cells. To understand the effects of low $[Ca]_o$ on the probability of transmitter release, we recorded miniature IPSC (mIPSC) frequency in either 1.5 or 1.1 mM $[Ca]_o$ in the presence of TTX (200 nM) to block all spike-associated transmitter release from presynaptic cells. Shifting from 1.5 to 1.1 mM $[Ca]_o$ lowered mIPSC frequency from 15 ± 2.9 Hz to 9.7 ± 1.5 Hz ($n = 10$, $p < 0.001$), reflecting an ~35% decrease in release probability at inhibitory synapses onto Purkinje cells (Fig. 7*A*,*B*), which is consistent with previous studies (King et al., 2001).

Based on these results, we predicted that sIPSCs would show a decrease in amplitude and frequency due to the decreased probability of release. We recorded sIPSCs in Purkinje cells in the presence of DNQX and DL-AP5 to block excitatory synaptic events and CGP55845 to block $GABA_B$ receptors. The use of a high CsCl internal solution to block potassium currents reversed the chloride gradient, revealing sIPSCs as inward current deflections. sIPSCs recorded in the slice preparation at 1.5 mM $[Ca]_o$ had variable amplitudes, attributed to synaptic events occurring at high frequency and originating from varying sites within the dendritic tree that lead to overlap and summation (Fig. 7*C*). Counter to our predictions, bath application of 1.1 mM $[Ca]_o$ substantially increased the proportion of large-amplitude sIPSCs ($n = 7$, $p < 0.001$, Kolmogorov–Smirnov test; Fig. 7*D*). Furthermore, the measured value of sIPSC frequency was not significantly different between 1.5 mM $[Ca]_o$ (26.6 ± 2.6 Hz, $n = 7$) and 1.1 mM $[Ca]_o$ (25 ± 4.7 Hz, $n = 7$, $p > 0.05$; Fig. 7*E*). Subsequent application of picrotoxin (50 μM) blocked nearly all synaptic currents (Fig. 7*D*,*E*), indicating that the majority of sIPSC activity was mediated by $GABA_A$ receptors.

In considering these results, we noted that large-amplitude events that may constitute simultaneous input from multiple sources would be difficult to distinguish from single events, potentially decreasing sIPSC frequency and increasing the measured proportion of large-amplitude events. We also reasoned that because probability of release decreased in 1.1 mM $[Ca]_o$ (Fig. 7*A*,*B*), the proportional increase in large-amplitude sIPSCs did not reflect an increase in spike-associated transmitter release. Our previous experiments also determined that stellate cell firing frequency increases in the presence of low $[Ca]_o$ (Fig. 4*A*). Therefore, we interpret these data to indicate that the increase in large-amplitude sIPSCs in 1.1 mM $[Ca]_o$ can be explained by an increase in interneuron firing frequency, resulting in a larger number of overlapping and summated events that could not be resolved to accurately determine net sIPSC frequency.

To determine the combined effect of these changes on Purkinje cell inhibitory tone, we measured the average charge transfer per second associated with sIPSCs (see Materials and Methods) (Fig. 6*F*). Under control conditions of 1.5 mM $[Ca]_o$, Purkinje cells received an average of 7.7 ± 1.1 pC ($n = 7$) from sIPSCs, with application of picrotoxin significantly reducing charge transfer (1.7 ± 0.3 pC, $n = 7$; Fig. 7*F*), indicating the primary role of GABAergic inputs. In contrast, application of 1.1 mM $[Ca]_o$ did not significantly change charge transfer (9.9 ± 2.6 pC, $n = 7$, $p > 0.05$; Fig. 7*F*). Therefore, these results suggest that charge transfer is maintained despite a decrease in release probability via a compensatory increase in stellate cell discharge.

To more closely examine the relationship between presynaptic spike discharge and postsynaptic inhibition in different levels of $[Ca]_o$, we performed dual recordings of synaptically connected stellate and Purkinje cells (Fig. 8). Presynaptic spikes in the recorded stellate cell that were correlated with postsynaptic IPSCs were identified by detecting an IPSC of at least 5 pA within 5 ms of a presynaptic spike peak (Fig. 8*A*). Spike-associated IPSCs were referred to as evoked IPSCs (eIPSCs) and used to create a spike-triggered average. If a presynaptic spike was not followed by an IPSC it was taken to reflect a failure of presynaptic transmission, as expected for the probabilistic nature of vesicle fusion and transmitter release. Finally, IPSCs with no clear association with spike discharge in the recorded presynaptic stellate cell were considered to be derived from other stellate or basket cells synapsing on the recorded Purkinje cell. Cell pairs that exhibited correlated presynaptic spikes and eIPSCs were encountered with a success rate of ~10–15% ($n = 5/42$ cells), as judged in *post hoc* analysis of spike-triggered responses in Purkinje cells. To improve calculations of the net influence of presynaptic spike discharge on postsynaptic inhibition in low $[Ca]_o$, stellate cells were held below threshold to prevent spontaneous discharge, and 20 current pulses were delivered to evoke repetitive firing (5–8 pA, 1 s duration, 5 s intervals; Fig. 8*A*).

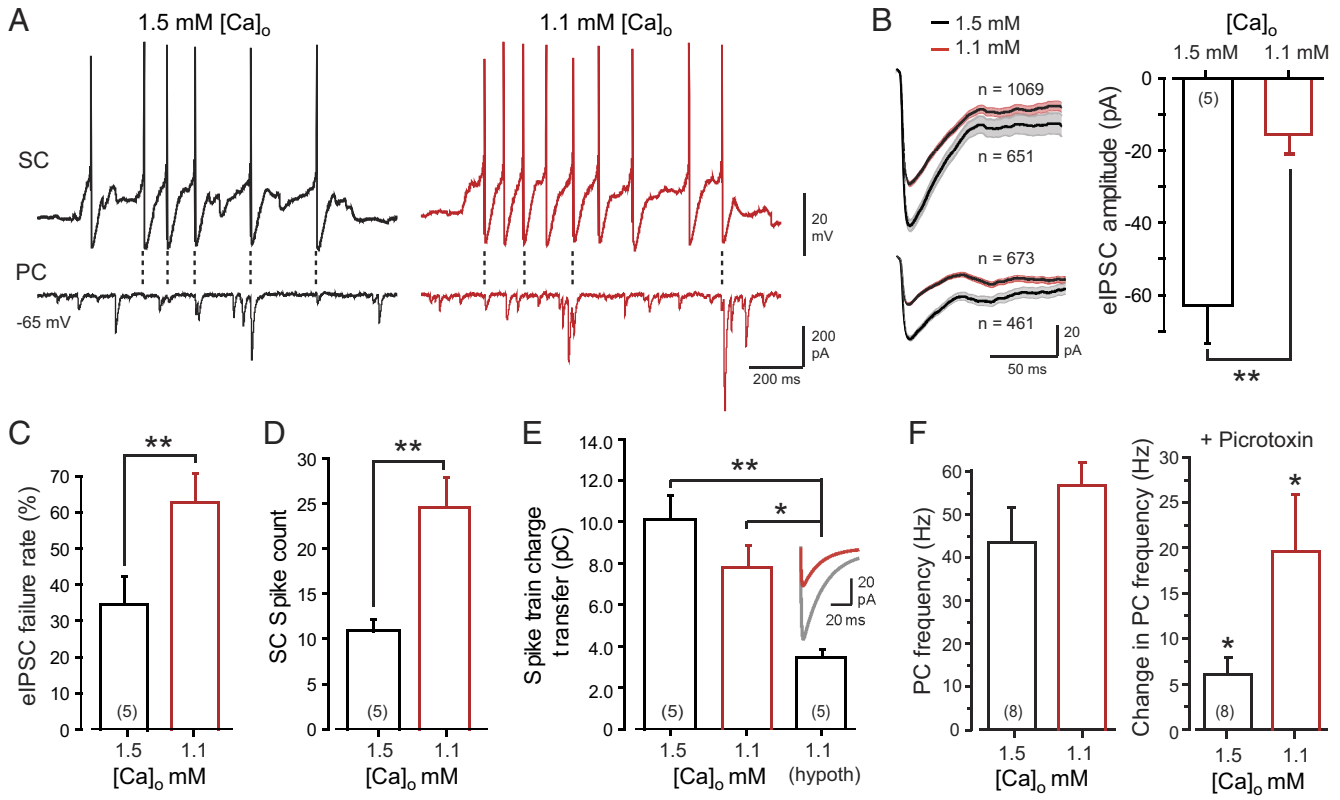

Figure 8. Inhibitory charge transfer of evoked IPSCs to Purkinje cells (PCs) is maintained in low $[Ca]_o$. Dual recordings of stellate (SC) and Purkinje cells were used to record presynaptic spike discharge and postsynaptic IPSCs in 1.5 or 1.1 mM $[Ca]_o$ in the presence of synaptic blockers. Stellate cells were held below threshold and presynaptic spike discharge evoked using 20 1 s current pulses while holding Purkinje cells at −65 mV to record inward IPSCs. ***A***, Recordings from a synaptically connected SCs and PCs. Dashed lines indicate stellate cell spikes giving rise to eIPSCs. ***B***, Superimposed spike-triggered averages of IPSCs and bar plots of eIPSC amplitudes in 1.5 or 1.1 mM $[Ca]_o$. Top traces include only eIPSCs directly associated with presynaptic spikes, while lower traces are all responses including transmission failures. SEM is indicated by shaded regions. ***C–E***, Bar plots of spike and eIPSC properties from identified stellate–Purkinje cell pairs in 1.5 and 1.1 mM $[Ca]_o$. Reducing $[Ca]_o$ from 1.5 to 1.1 mM significantly increases eIPSC failure rate in ***C*** and increases current-evoked stellate cell spike count in ***D***. ***E***, Mean values for spike train charge transfer from stellate to Purkinje cells in 1.5 and 1.1 mM $[Ca]_o$, calculated as the product of spike count in ***D*** and fits (inset) to the mean eIPSCs shown in lower records of ***B***. Charge transfer in 1.1 mM $[Ca]_o$ was calculated for both the actual spike count and for a hypothetical situation (1.1 hypoth) where spike count did not change from that recorded in 1.5 mM $[Ca]_o$. ***F***, Bar plots of Purkinje cell spontaneous firing rates during on-cell recordings. The rate of Purkinje cell firing is not significantly different during perfusion of 1.5 or 1.1 mM $[Ca]_o$. Addition of picrotoxin (50 μM) reveals that the level of Purkinje cell excitability would be significantly higher in 1.1 mM $[Ca]_o$ without the associated increase in GABAergic inhibition in the network. Sample values are shown in brackets within bar plots. *$p < 0.05$; **$p < 0.01$.

Spike-triggered averages were calculated both with and without transmission failures to determine the effect on lowering $[Ca]_o$ on eIPSCs. When failures were not included, eIPSC amplitudes decreased from −92.8 ± 4.1 pA in 1.5 mM $[Ca]_o$ to −62.8 ± 10.6 pA in 1.1 mM $[Ca]_o$ ($n = 5$, $p < 0.05$; Fig. 8*B*, top traces). When all postsynaptic responses (regardless of failure) were included in the average as a measure of overall inhibitory influence, it was revealed that lowering $[Ca]_o$ decreased the net amplitude of spike-related postsynaptic inhibitory events from −62.8 ± 10.6 pA in 1.5 mM $[Ca]_o$ to −15.6 ± 4.6 pA 1.1 mM $[Ca]_o$ ($n = 5976$ spikes over 5 cells, $p < 0.01$; Fig. 8*B*, right, bottom traces). This large decrease in eIPSC amplitude was due to an increase in failure rate at the stellate cell to Purkinje cell synapse from 34.6 ± 7.7% in 1.5 mM $[Ca]_o$ to 62.8 ± 8.0% in 1.1 mM $[Ca]_o$ ($n = 5$, $p < 0.01$; Fig. 8*C*).

The increase in failure rate of stellate cell synaptic transmission in 1.1 mM $[Ca]_o$ would predict that the level of stellate cell-mediated inhibition will be diminished during repetitive synaptic input that decreases $[Ca]_o$ *in vivo*. On the other hand, the gain of stellate firing is increased in 1.1 mM $[Ca]_o$ through the action of the Ca_v3–K_v4 complex, suggesting a mechanism to counteract decreased synaptic efficacy at stellate to Purkinje cell synapses. Indeed, the average number of spikes evoked by a 1 s current step in stellate cells increased from 10.9 ± 1.3 spikes in control to 24.6 ± 3.3 spikes in 1.1 mM $[Ca]_o$ (Fig. 8*D*; $n = 5$, $p < 0.01$). We thus examined the combined effects of an increased failure rate of synaptic events, decreased IPSC amplitude, and an increase in spike count on the overall charge transfer. Charge transfer was compared under three conditions: normal gain of stellate cell output in 1.5 mM $[Ca]_o$, increased gain of stellate cell output in 1.1 mM $[Ca]_o$, and a hypothetical case where stellate cell gain was unchanged in 1.1 mM $[Ca]_o$. To calculate charge transfer, we used simulated IPSCs for 1.5 and 1.1 mM $[Ca]_o$ conditions, created by fitting the spike-triggered averages (including failures) from a representative cell. The charge transfer for a 1 s presynaptic spike train was calculated by multiplying the area under the simulated IPSC by the average number of spikes per second for each of the three conditions.

With an average of 11 spikes for a 1 s current step in 1.5 mM $[Ca]_o$ ($n = 5$), charge transfer was predicted to be 9.7 ± 1.2 pC (Fig. 8*E*). Repeating these calculations for 1.1 mM $[Ca]_o$ revealed that spike train charge transfer was maintained in the lower calcium condition when the number of spikes increased to 25 spikes/s (7.8 ± 1.0 pC, $n = 5$, $p > 0.05$; Fig. 8*E*). However, in a hypothetical situation where the number of spikes per unit time was unchanged in 1.1 mM $[Ca]_o$ from that in 1.5 mM $[Ca]_o$ (11

spikes/s), the predicted spike train charge transfer was greatly reduced to 3.4 ± 0.4 pC ($n = 5$; Fig. 8*E*), a value that is significantly different from both the 1.5 and 1.1 mM $[Ca]_o$ conditions ($p < 0.01$ for both comparisons). Collectively, these data indicate that decreased synaptic efficacy in low $[Ca]_o$ is overcome by way of a Ca_v3–K_v4 complex-mediated increase in stellate cell gain of firing.

An adaptive response of the inhibitory network restrains Purkinje cell firing

These results would predict that at the network level, the rate of Purkinje cell firing should be maintained in homeostatic manner despite fluctuations in extracellular ionic concentrations during synaptic input. To directly test this, we used on-cell recordings to monitor the rate of spontaneous Purkinje cell firing in response to modulations of $[Ca]_o$ and $[K]_o$ characteristic of physiologically relevant inputs. In all of these recordings, DL-AP5 (25 μM) and DNQX (10 μM) were included in the bath to block excitatory synaptic transmission. Cells were recorded from animals at P18–P20 to reduce the probability of inducing trimodal activity (McKay and Turner, 2005), and were excluded if trimodal activity was detected. Cells were recorded in an initial control solution of 1.5 mM $[Ca]_o$ and then perfused with 1.1 mM $[Ca]_o$, and finally 50 μM picrotoxin to block all GABAergic inputs to assess the relative influence of the inhibitory network on Purkinje cell firing rate under each condition. In 1.5 mM $[Ca]_o$ Purkinje cells discharged at a rate of 43.6 ± 7.8 Hz ($n = 8$), with no significant increase in firing rate in the presence of lowered $[Ca]_o$ (Fig. 8*F*). Perfusing picrotoxin on cells maintained in 1.5 mM $[Ca]_o$ revealed a modest but significant mean increase in firing rate of ~5 Hz. However, in the presence of 1.1 mM $[Ca]_o$, picrotoxin unmasked a significant increase in Purkinje cell firing of ~20–25 Hz over the baseline rate of firing ($p < 0.05$; Fig. 8*F*). To fully test the influence of ionic factors that can change during repetitive synaptic inputs, these tests were repeated for exposures to both 1.1 mM $[Ca]_o$ and 4.0 mM $[K]_o$, with the same results (data not shown).

These data indicate that the increase in activity of inhibitory interneurons in 1.1 mM $[Ca]_o$ acts to lower the excitability and firing rate of Purkinje cells in the order of ~40% compared to the level that would be encountered without the inhibitory network. The reason for the increase in firing rate of Purkinje cells in the absence of GABAergic inhibition was not fully determined here. However, it does not relate to a Ca_v3–K_v4 interaction in Purkinje cells, as rat Purkinje cells have not been found to express K_v4 current (our unpublished observations). It could instead be due to an increase in excitability caused by decreased activation of calcium-dependent AHPs in Purkinje cells (Hosy et al., 2011; Engbers et al., 2012). These data are then consistent with a compensatory increase in the firing rate of stellate cells via the Ca_v3–K_v4 complex to suppress an increase in Purkinje cell excitability that would occur in low $[Ca]_o$. This adaptive form of inhibitory control then acts in a homeostatic fashion to limit nonspecific increases in Purkinje cell excitability during repetitive afferent activity.

Discussion

Early measurements of $[Ca]_o$ with ion-selective electrodes reported that peripheral stimulation of afferent inputs to cerebellum rapidly reduce $[Ca]_o$ in the order of 0.4 mM or more in the molecular layer (Stöckle and ten Bruggencate, 1980). Subsequent studies established that even minimal rates of spike invasion and transmitter release reliably deplete $[Ca]_o$ in a synaptic cleft. Thus, experiments employing ion-selective electrodes (Heinemann et al., 1977; Nicholson et al., 1978; Stöckle and ten Bruggencate, 1978; Torres et al., 2012), dual patch recordings (Borst and Sakmann, 1999; Stanley, 2000), two-photon imaging (Rusakov and Fine, 2003), and modeling (Egelman and Montague, 1999; Wiest et al., 2000; King et al., 2001) all report measureable decreases in $[Ca]_o$ or its predicted consequence on presynaptic and postsynaptic responses during physiological rates of activation. The direct recordings of I_T in stellate cells provided here now confirm that repetitive climbing fiber stimulation reduces the driving force for calcium in a manner consistent with a decrease in $[Ca]_o$.

Stimulus-induced reductions in $[Ca]_o$ seem counterintuitive in that the efficacy of transmitter release will be reduced and circuit function altered in the act of processing incoming signals. The mechanism by which cerebellar circuit function is maintained during stimulus-induced changes in membrane currents had not been identified. Our data now provide evidence that the Ca_v3–K_v4 complex alters stellate cell excitability to maintain inhibitory charge transfer to Purkinje cells during a reduction in $[Ca]_o$.

The Ca_v3–K_v4 complex as a calcium sensor

Our tests in both stellate cells and tsA-201 cells reveal that decreases in $[Ca]_o$ of 0.4 mM are sufficient to shift the V_h of A-type current toward negative potentials, reducing the availability of K_v4 current. Indeed, the steepest component of a dose–response curve for $[Ca]_o$ I_A V_h was situated directly within the range of $[Ca]_o$ changes reported *in vivo* (Nicholson et al., 1978; Stöckle and ten Bruggencate, 1978, 1980). Both the shifts in V_h and increases in gain of stellate cell firing were KChIP3-dependent, as expected for the Ca_v3–K_v4 interaction. These data indicate that the Ca_v3–K_v4 complex can effectively act as a novel sensor for $[Ca]_o$.

Calcium sensors that can influence neuronal excitability have been reported previously. Nevertheless, each of these differ from the calcium sensing capabilities of the Ca_v3–K_v4 complex. A calcium-sensing receptor (CaSR) is widely expressed (Ruat et al., 1995; Washburn et al., 1999; Bandyopadhyay et al., 2010), but CaSR immunolabel is not detected in stellate cells (Ruat et al., 1995), and activation of CaSR requires an increase in $[Ca]_o$ (Washburn et al., 1999; Lu et al., 2010). A sodium-conducting leak channel (NALCN) can increase neuronal excitability when $[Ca]_o$ is lowered (Lu et al., 2010), but the low calcium-induced increase in stellate cell firing is occluded by mibefradil (500 nM), which does not affect NALCN channels (Lu et al., 2007). TRPM7 channels activate in low $[Ca]_o$ but with an IC_{50} of 4.1 μM $[Ca]_o$ (Li et al., 2007; Wei et al., 2007), well below the range of $[Ca]_o$ tested here. Although low calcium-induced increases in excitability can involve charge-screening effects (Formenti et al., 2001), we minimized this by balancing the concentration of extracellular divalent ions with elevated $[Mg^{2+}]_o$. Furthermore, any charge-screening effects are predicted to occur at the extracellular face, while the effects here were occluded by internal infusion of a KChIP3 antibody. Therefore, the changes in stellate cell excitability when $[Ca]_o$ is decreased can be attributed to the Ca_v3–K_v4 complex acting as a sensor for changes in $[Ca]_o$.

Inhibitory control of cerebellar output during changes in $[Ca]_o$

Stellate cells form an axonal network in the molecular layer that is highly effective in controlling Purkinje cell excitability and spike output (Callaway et al., 1995; Häusser and Clark, 1997; Mann-

Metzer and Yarom, 1999; Barmack and Yakhnitsa, 2008). The effects of a decrease in $[Ca]_o$ in the molecular layer on cell excitability and synaptic transmission could then disrupt cerebellar output. This could particularly be the case for climbing fiber input that activates a large-amplitude calcium-dependent complex spike that conducts throughout the Purkinje cell dendritic tree (Llinás and Sugimori, 1980a, b; Kitamura and Häusser, 2011), providing a large postsynaptic sink for calcium from the extracellular space. In addition, glutamate spillover during high-frequency climbing fiber input can reduce GABA release from presynaptic terminals of molecular layer interneurons (Satake et al., 2000; Rusakov et al., 2005), while endocannabinoid release from Purkinje cells can reduce stellate cell firing (Kreitzer et al., 2002). It thus seems difficult to predict how inhibitory tone is maintained on Purkinje cells during repetitive climbing fiber input. Despite this, careful analyses of the role of cerebellar interneurons suggest that stellate cells are the primary elements mediating a climbing fiber-induced reduction of Purkinje cell simple spike discharge (Barmack and Yakhnitsa, 2008).

The actions of a Ca_v3–K_v4 complex now reveals a mechanism by which inhibitory charge transfer can be maintained between stellate and Purkinje cells during repetitive climbing fiber input. Our data indicate that the Ca_v3–K_v4 complex allows stellate cells to respond to a decrease in $[Ca]_o$ that will occur when climbing fiber input activates a complex spike in nearby Purkinje cell dendrites. Ultramicrographs of K_v4 channel distribution (Kollo et al., 2006) indicate that K_v4 channels are concentrated between stellate cells and climbing fiber boutons and within 300 nm of climbing fiber synapses on Purkinje cell dendrites, increasing the likelihood of being positioned within the zone of calcium depletion. Indeed, the change in $[Ca]_o$ can be expected to be even greater within the narrow space available in the junction that exists between climbing fiber terminals and stellate cells (Kollo et al., 2006; Syková and Nicholson, 2008). Our recordings of I_T in stellate cells established that a change in driving force for calcium is readily detected even *in vitro* for bath perfusions of different $[Ca]_o$ (Fig. 1*D*), with a concomitant decrease in I_T and I_A density during climbing fiber stimulation (Fig. 2). In fact, repetitive climbing fiber activation was closely correlated with a reduction in both I_T and I_A in stellate cells, with the effect on I_A blocked when $[Ca]_o$ was raised to 2.2 mM. All these results are consistent with the Ca_v3–K_v4 complex responding to changes in $[Ca]_o$ that in turn reduce I_A availability through its action on the K_v4 voltage-dependence of inactivation.

A reduction in I_A availability is important to functional output because it is associated with a decrease in spike threshold and increase in spike frequency in stellate cells. An increase in stellate firing rate would be predicted to elevate the level of GABAergic inhibition onto Purkinje cells, reducing dendritic calcium spikes and modifying Purkinje cell output. Recordings in Purkinje cells confirmed that the net activity of sIPSCs was substantially increased when $[Ca]_o$ was lowered from 1.5 to 1.1 mM. However, paired recordings also revealed a decrease in the amplitude and increase in the probability of failure of eIPSCs in lowered $[Ca]_o$. A decrease of only 0.4 mm $[Ca]_o$ is then sufficient to reduce the probability of transmitter release and efficacy of transmission between stellate and Purkinje cells (Borst and Sakmann, 1999; Rusakov and Fine, 2003). Despite this, the elevated rate of stellate cell firing in reduced $[Ca]_o$ almost fully offset the associated decrease in IPSC influence. The ability for an enhanced level of inhibition to act at the circuit level to restrain Purkinje cell firing during reductions in $[Ca]_o$ was apparent when the relative effects of picrotoxin on Purkinje cell output were compared under control and test conditions (Fig. 8*F*).

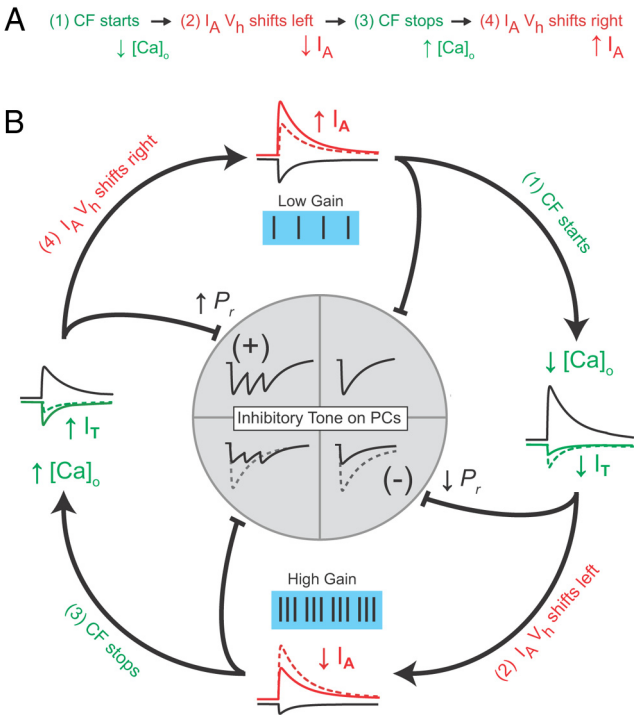

Figure 9. Diagrammatic representations of the sequence of events proposed for climbing fiber (CF)-induced reductions in $[Ca]_o$, stellate cell ionic currents, and adaptive inhibitory control of Purkinje cell (PC) excitability. ***A***, A text-based sequence of events related to CF-induced shifts in $[Ca]_o$ and I_T and I_A in stellate cells. ***B***, A schematic diagram and flow chart of the entire sequence of events underlying adaptive inhibition by stellate cells to maintain a homeostatic balance of inhibitory charge transfer (tone) on Purkinje cells during repetitive CF inputs. Text in green indicates CF-induced changes in $[Ca]_o$ and I_T, and text in red indicates events that lead to shifts in I_A availability in stellate cells. The center circle indicates the change in amplitude and pattern of GABAergic IPSPs in Purkinje cells. Under control conditions, I_A availability is high and stellate cell excitability is low (low gain). Repetitive CF input reduces $[Ca]_o$ and I_T, leading to a decrease in I_A availability through the Ca_v3–K_v4 complex (V_h shifts left). An associated increase in stellate cell firing (high gain) compensates for a reduction in release probability (P_r) when $[Ca]_o$ decreases. When CF input stops, $[Ca]_o$ and I_A V_h return to normal, and stellate cell excitability is reduced when I_A availability increases by way of the Ca_v3–K_v4 complex.

Adaptive control of inhibition

Together the data indicate that cerebellar circuit function can be maintained in the face of synaptically evoked reductions in $[Ca]_o$ by the actions of a Ca_v3–K_v4 complex that adaptively adjusts the level of inhibition to maintain inhibitory charge transfer to Purkinje cells. A schematic representation of the events we propose accompany repetitive climbing fiber input and its effects on $[Ca]_o$, I_T and I_A density, and adaptive control of inhibitory charge transfer to Purkinje cells is summarized in Figure 9. Moreover, by positioning numerous stellate cells in different regions of the Purkinje cell dendritic tree, the Ca_v3–K_v4 complex could provide local (single stellate cells) or more global (multiple stellate cells) control of dendritic activity depending on the extent of evoked activity in the dendritic arbor. This will be important in providing a homeostatic balance of inhibition to maintain Purkinje cell output at a level that will allow an appropriate response in the course of processing afferent inputs. Direct recordings of I_T suggest that a synaptically evoked decrease in $[Ca]_o$ can recover within ~1 s *in vitro*, while ion-selective electrodes suggest that full recovery of $[Ca]_o$

in the extracellular space *in vivo* may be even longer (Nicholson et al., 1978; Stöckle and ten Bruggencate, 1980). Note that a timeline of only seconds differs substantially from other forms of homeostatic plasticity that require hours or days of intervention to invoke long-term shifts in inhibitory function (Wenner, 2011). Given the widespread expression of Ca_v3 and K_v4 channels, we predict that the Ca_v3–K_v4 complex will be an integral part of inhibitory control in many other central neural circuits.

References

Anderson D, Rehak R, Hameed S, Mehaffey WH, Zamponi GW, Turner RW (2010a) Regulation of the $K_v4.2$ complex by CaV3.1 calcium channels. Channels (Austin) 4:163–167. Medline

Anderson D, Mehaffey WH, Iftinca M, Rehak R, Engbers JD, Hameed S, Zamponi GW, Turner RW (2010b) Regulation of neuronal activity by Cav3-Kv4 channel signaling complexes. Nat Neurosci 13:333–337. CrossRef Medline

Bandyopadhyay S, Tfelt-Hansen J, Chattopadhyay N (2010) Diverse roles of extracellular calcium-sensing receptor in the central nervous system. J Neurosci Res 88:2073–2082. CrossRef Medline

Barmack NH, Yakhnitsa V (2008) Functions of interneurons in mouse cerebellum. J Neurosci 28:1140–1152. CrossRef Medline

Borst JG, Sakmann B (1999) Depletion of calcium in the synaptic cleft of a calyx-type synapse in the rat brainstem. J Physiol 521:123–133. Medline

Brown KM, Sugihara I, Shinoda Y, Ascoli GA (2012) Digital morphometry of rat cerebellar climbing fibers reveals distinct branch and bouton types. J Neurosci 32:14670–14684. CrossRef Medline

Bruggencate GT, Nicholson C, Stöckle H (1976) Climbing fiber evoked potassium release in cat cerebellum. Pflugers Arch 367:107–109. CrossRef Medline

Burgoyne RD (2007) Neuronal calcium sensor proteins: generating diversity in neuronal Ca2+ signalling. Nat Rev Neurosci 8:182–193. CrossRef Medline

Callaway JC, Lasser-Ross N, Ross WN (1995) IPSPs strongly inhibit climbing fiber-activated [Ca2+]i increases in the dendrites of cerebellar Purkinje neurons. J Neurosci 15:2777–2787. Medline

Carrasquillo Y, Burkhalter A, Nerbonne JM (2012) A-type K+ channels encoded by Kv4.2, Kv4.3 and Kv1.4 differentially regulate intrinsic excitability of cortical pyramidal neurons. J Physiol 590:3877–3890. CrossRef Medline

Connor JA, Stevens CF (1971a) Voltage clamp studies of a transient outward membrane current in gastropod neural somata. J Physiol 213:21–30. Medline

Connor JA, Stevens CF (1971b) Prediction of repetitive firing behaviour from voltage clamp data on an isolated neurone soma. J Physiol 213:31–53. Medline

Crepel F, Daniel H (2007) Developmental changes in agonist-induced retrograde signaling at parallel fiber-Purkinje cell synapses: role of calcium-induced calcium release. J Neurophysiol 98:2550–2565. CrossRef Medline

Dorval AD, Christini DJ, White JA (2001) Real-Time linux dynamic clamp: a fast and flexible way to construct virtual ion channels in living cells. Ann Biomed Eng 29:897–907. CrossRef Medline

Egelman DM, Montague PR (1999) Calcium dynamics in the extracellular space of mammalian neural tissue. Biophys J 76:1856–1867. CrossRef Medline

Engbers JD, Anderson D, Asmara H, Rehak R, Mehaffey WH, Hameed S, McKay BE, Kruskic M, Zamponi GW, Turner RW (2012) Intermediate conductance calcium-activated potassium channels modulate summation of parallel fiber input in cerebellar Purkinje cells. Proc Natl Acad Sci U S A 109:2601–2606. CrossRef Medline

Formenti A, De Simoni A, Arrigoni E, Martina M (2001) Changes in extracellular Ca2+ can affect the pattern of discharge in rat thalamic neurons. J Physiol 535:33–45. CrossRef Medline

Gasparini F, Lingenhöhl K, Stoehr N, Flor PJ, Heinrich M, Vranesic I, Biollaz M, Allgeier H, Heckendorn R, Urwyler S, Varney MA, Johnson EC, Hess SD, Rao SP, Sacaan AI, Santori EM, Veliçelebi G, Kuhn R (1999) 2-Methyl-6-(phenylethynyl)-pyridine (MPEP), a potent, selective and systemically active mGlu5 receptor antagonist. Neuropharmacology 38:1493–1503. CrossRef Medline

Gatley SJ, Gifford AN, Volkow ND, Lan R, Makriyannis A (1996) 123I-labeled AM251: a radioiodinated ligand which binds *in vivo* to mouse brain cannabinoid CB1 receptors. Eur J Pharmacol 307:331–338. CrossRef Medline

Hámori J, Szentágothai J (1980) Lack of evidence of synaptic contacts by climbing fibre collaterals to basket and stellate cells in developing rat cerebellar cortex. Brain Res 186:454–457. CrossRef Medline

Häusser M, Clark BA (1997) Tonic synaptic inhibition modulates neuronal output pattern and spatiotemporal synaptic integration. Neuron 19:665–678. CrossRef Medline

Heinemann U, Lux HD, Gutnick MJ (1977) Extracellular free calcium and potassium during paroxsmal activity in the cerebral cortex of the cat. Exp Brain Res 27:237–243. Medline

Hoffman DA, Magee JC, Colbert CM, Johnston D (1997) K+ channel regulation of signal propagation in dendrites of hippocampal pyramidal neurons. Nature 387:869–875. CrossRef Medline

Hosy E, Piochon C, Teuling E, Rinaldo L, Hansel C (2011) SK2 channel expression and function in cerebellar Purkinje cells. J Physiol 589:3433–3440. CrossRef Medline

Jörntell H, Ekerot CF (2003) Receptive field plasticity profoundly alters the cutaneous parallel fiber synaptic input to cerebellar interneurons *in vivo*. J Neurosci 23:9620–9631. Medline

Khaliq ZM, Bean BP (2008) Dynamic, nonlinear feedback regulation of slow pacemaking by A-type potassium current in ventral tegmental area neurons. J Neurosci 28:10905–10917. CrossRef Medline

King RD, Wiest MC, Montague PR (2001) Extracellular calcium depletion as a mechanism of short-term synaptic depression. J Neurophysiol 85:1952–1959. Medline

Kitamura K, Häusser M (2011) Dendritic calcium signaling triggered by spontaneous and sensory-evoked climbing fiber input to cerebellar Purkinje cells *in vivo*. J Neurosci 31:10847–10858. CrossRef Medline

Knöpfel T (2007) Two new non-competitive mGlu1 receptor antagonists are potent tools to unravel functions of this mGlu receptor subtype. Br J Pharmacol 151:723–724. CrossRef Medline

Kollo M, Holderith NB, Nusser Z (2006) Novel subcellular distribution pattern of A-type K+ channels on neuronal surface. J Neurosci 26:2684–2691. CrossRef Medline

Kreitzer AC, Carter AG, Regehr WG (2002) Inhibition of interneuron firing extends the spread of endocannabinoid signaling in the cerebellum. Neuron 34:787–796. CrossRef Medline

Li M, Du J, Jiang J, Ratzan W, Su LT, Runnels LW, Yue L (2007) Molecular determinants of Mg2+ and Ca2+ permeability and pH sensitivity in TRPM6 and TRPM7. J Biol Chem 282:25817–25830. CrossRef Medline

Llinás R, Sugimori M (1980a) Electrophysiological properties of *in vitro* Purkinje cell somata in mammalian cerebellar slices. J Physiol 305:171–195. Medline

Llinás R, Sugimori M (1980b) Electrophysiological properties of *in vitro* Purkinje cell dendrites in mammalian cerebellar slices. J Physiol 305:197–213. Medline

Lu B, Su Y, Das S, Liu J, Xia J, Ren D (2007) The neuronal channel NALCN contributes resting sodium permeability and is required for normal respiratory rhythm. Cell 129:371–383. CrossRef Medline

Lu B, Zhang Q, Wang H, Wang Y, Nakayama M, Ren D (2010) Extracellular calcium controls background current and neuronal excitability via an UNC79-UNC80-NALCN cation channel complex. Neuron 68:488–499. CrossRef Medline

Mann-Metzer P, Yarom Y (1999) Electrotonic coupling interacts with intrinsic properties to generate synchronized activity in cerebellar networks of inhibitory interneurons. J Neurosci 19:3298–3306. Medline

McCreery DB, Agnew WF (1983) Changes in extracellular potassium and calcium concentration and neural activity during prolonged electrical stimulation of the cat cerebral cortex at defined charge densities. Exp Neurol 79:371–396. CrossRef Medline

McKay BE, Turner RW (2005) Physiological and morphological development of the rat cerebellar Purkinje cell. J Physiol 567:829–850. CrossRef Medline

Molineux ML, Fernandez FR, Mehaffey WH, Turner RW (2005) A-type and T-type currents interact to produce a novel spike latency-voltage relationship in cerebellar stellate cells. J Neurosci 25:10863–10873. CrossRef Medline

Molineux ML, McRory JE, McKay BE, Hamid J, Mehaffey WH, Rehak R, Snutch TP, Zamponi GW, Turner RW (2006) Specific T-type calcium channel isoforms are associated with distinct burst phenotypes in deep

cerebellar nuclear neurons. Proc Natl Acad Sci U S A 103:5555–5560. CrossRef Medline

Nicholson C, ten Bruggencate G, Stöckle H, Steinberg R (1978) Calcium and potassium changes in extracellular microenvironment of cat cerebellar cortex. J Neurophysiol 41:1026–1039. Medline

Nilsen A, England PM (2007) A subtype-selective, use-dependent inhibitor of native AMPA receptors. J Am Chem Soc 129:4902–4903. CrossRef Medline

Nishiyama H, Fukaya M, Watanabe M, Linden DJ (2007) Axonal motility and its modulation by activity are branch-type specific in the intact adult cerebellum. Neuron 56:472–487. CrossRef Medline

Norris AJ, Nerbonne JM (2010) Molecular dissection of I(A) in cortical pyramidal neurons reveals three distinct components encoded by Kv4.2, Kv4.3, and Kv1.4 alpha-subunits. J Neurosci 30:5092–5101. CrossRef Medline

Norris AJ, Foeger NC, Nerbonne JM (2010) Interdependent roles for accessory KChIP2, KChIP3, and KChIP4 subunits in the generation of Kv4-encoded IA channels in cortical pyramidal neurons. J Neurosci 30:13644–13655. CrossRef Medline

Ruat M, Molliver ME, Snowman AM, Snyder SH (1995) Calcium sensing receptor: molecular cloning in rat and localization to nerve terminals. Proc Natl Acad Sci U S A 92:3161–3165. CrossRef Medline

Rusakov DA, Fine A (2003) Extracellular Ca2+ depletion contributes to fast activity-dependent modulation of synaptic transmission in the brain. Neuron 37:287–297. CrossRef Medline

Rusakov DA, Saitow F, Lehre KP, Konishi S (2005) Modulation of presynaptic Ca2+ entry by AMPA receptors at individual GABAergic synapses in the cerebellum. J Neurosci 25:4930–4940. CrossRef Medline

Satake S, Saitow F, Yamada J, Konishi S (2000) Synaptic activation of AMPA receptors inhibits GABA release from cerebellar interneurons. Nat Neurosci 3:551–558. CrossRef Medline

Stanley EF (2000) Presynaptic calcium channels and the depletion of synaptic cleft calcium ions. J Neurophysiol 83:477–482. Medline

Stöckle H, ten Bruggencate G (1978) Climbing fiber-mediated rhythmic modulations of potassium and calcium in cat cerebellar cortex. Exp Neurol 61:226–230. CrossRef Medline

Stöckle H, ten Bruggencate G (1980) Fluctuation of extracellular potassium and calcium in the cerebellar cortex related to climbing fiber activity. Neuroscience 5:893–901. CrossRef Medline

Syková E, Nicholson C (2008) Diffusion in brain extracellular space. Physiol Rev 88:1277–1340. CrossRef Medline

Szapiro G, Barbour B (2007) Multiple climbing fibers signal to molecular layer interneurons exclusively via glutamate spillover. Nat Neurosci 10:735–742. CrossRef Medline

Talbot MJ, Sayer RJ (1996) Intracellular QX-314 inhibits calcium currents in hippocampal CA1 pyramidal neurons. J Neurophysiol 76:2120–2124. Medline

Torres A, Wang F, Xu Q, Fujita T, Dobrowolski R, Willecke K, Takano T, Nedergaard M (2012) Extracellular Ca(2)(+) acts as a mediator of communication from neurons to glia. Sci Signal 5:ra8. CrossRef Medline

Washburn DL, Smith PM, Ferguson AV (1999) Control of neuronal excitability by an ion-sensing receptor (correction of anion-sensing). Eur J Neurosci 11:1947–1954. CrossRef Medline

Wei WL, Sun HS, Olah ME, Sun X, Czerwinska E, Czerwinski W, Mori Y, Orser BA, Xiong ZG, Jackson MF, Tymianski M, MacDonald JF (2007) TRPM7 channels in hippocampal neurons detect levels of extracellular divalent cations. Proc Natl Acad Sci U S A 104:16323–16328. CrossRef Medline

Wenner P (2011) Mechanisms of GABAergic homeostatic plasticity. Neural Plast 2011:489470. Medline

Wiest MC, Eagleman DM, King RD, Montague PR (2000) Dendritic spikes and their influence on extracellular calcium signaling. J Neurophysiol 83:1329–1337. Medline